molecular pharmaceutics

Article

Cite This: Mol. Pharmaceutics XXXX, XXX, XXX−XXX

Nanoformulation of EPZ011989 Attenuates EZH2−c-Myb Epigenetic Interaction by Proteasomal Degradation in Acute Myeloid Leukemia

Babita Kaundal, Anup K. Srivastava, Atul Dev, Soni Jignesh Mohanbhai, Surajit Karmakar, and Subhasree Roy Choudhury*

Institute of Nano Science and Technology, Phase-10, Mohali (Habitat Center), Punjab 160062, India

Supporting Information

ABSTRACT: Acute myeloid leukemia (AML) is a malignant disorder of hematopoietic progenitor cells with a poor prognosis of 26% of patients surviving 5 years after diagnosis. Poor bioavailability and solubility are significant factors limiting the efficacy of chemopreventive agents. In AML, the epigenetic regulator polycomb group of protein member EZH2 is highly expressed and is essential for the survival of leukemic cells. An EZH2-specific inhibitor, EPZ011989, encapsulated in human serum albumin nanoparticles (HSANPs) was synthesized for the first time via the desolvation method. The noncovalent interactions between EPZ011989 and HSANPs in nanocomposites facilitating the efficient loading and sustainable release of the drug showed enhanced cellular uptake and nuclear localization of EPZ011989-loaded HSANPs in human AML cell lines. The reduction of cell viability, colony formation inhibition, cell cycle arrest at the G2/M phase, and cell proliferation assay promoting apoptosis through the loss of mitochondrial homeostasis exerting antileukemic activity were evident. The real-time polymerase chain reaction (PCR) and western blot-based studies showed that the present nanoformulation reduces the level of PcG proteins, including EZH2, BMI-1, etc. This downregulation is associated with reduced H3K27me3 and H2AK119ub modifications conferring chromatin compaction. The immunoprecipitation study showed the physical interaction of EZH2 and c-Myb can be linked to the regulation of leukemogenesis. Further investigation revealed the mechanism of EZH2 and c-Myb downregulation via ubiquitination and proteasomal degradation pathway, confirmed by using proteasome inhibitor, suggesting the key role of proteasomal degradation machinery. Moreover, c-Myb interacted with the EZH2 promoter, which is evident by the chromatin immunoprecipitation assay and siRNA silencing. Furthermore, the formulation of EPZ011989 in HSANPs improved its biodistribution in vivo and showed excellent aqueous dispersibility and biocompatibility. In vivo studies further showed that EPZ011989-loaded HSANPs reduce the expression of $CD11b^+$ and $CD45^+$ markers in immunophenotyping from peripheral blood and bone marrow in engrafted nude mice. Targeted depletion of EZH2 alleviated the disease progression in nude mice and prolonged their survival. The findings provide valuable experimental evidence for the targeted epigenetic therapy of AML. The present results demonstrate an epigenetic regulation-based superior antileukemic therapy.

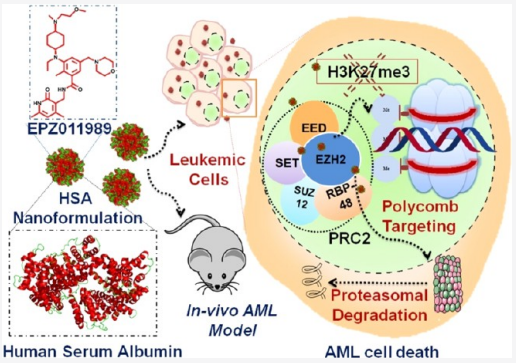

KEYWORDS: *epigenetics, methyltransferase, EPZ011989, nanoformulation, acute myeloid leukemia*

1. INTRODUCTION

Acute myeloid leukemia (AML) is a highly complex and heterogeneous disorder arising from multiple and dynamic mutations in the primitive hematopoietic stem or progenitor cells.[1,2] The underlying dynamic cytogenetic abnormality leads to immature and abnormal differentiation of myeloid effector cells.[3] These abnormalities lead to bone marrow failure and other systemic consequences that are a prerequisite to early prognosis and treatments.[4−6] The risk of AML occurrence is predominating in old age, with an incidence rate of nearly 14 per 100 000.[7,8]

The use of immunotherapeutic agents and targeting of biochemical pathways have not substantially evolved AML therapy and limits the five-year overall survival to 26% of the afflicted population.[9−11] Mutational landscape and genomic instability studies revealed the involvement of essential epigenetic regulation mechanisms in the early pathogenesis of AML.[12] These genetic and epigenetic alterations perturb the key processes of proliferation, differentiation, apoptosis, and gene transcription, resulting in leukemogenesis. The essential epigenetic systems involved in heritable repression of gene activity are the polycomb group (PcG) proteins, which play a vital role in the initiation and maintenance of gene silencing through histone modifications.[13,14] PcG proteins belong to two major complexes, polycomb repressive complexes 1 and 2 (PRC1 and PRC2). The histone methyltransferase enhancer of zeste homologue 2 (EZH2), a methyltransferase component of

Received: October 14, 2019
Revised: December 18, 2019
Accepted: December 18, 2019

DOI: 10.1021/acs.molpharmaceut.9b01071
Mol. Pharmaceutics XXXX, XXX, XXX−XXX

Scheme 1. Schematic Representing the Mechanism of EPZ011989-Loaded HSA Nanoparticle that Allows Transcription of Tumor Suppressor gene EZH2 Deactivation by the Proteasome-Mediated Pathway

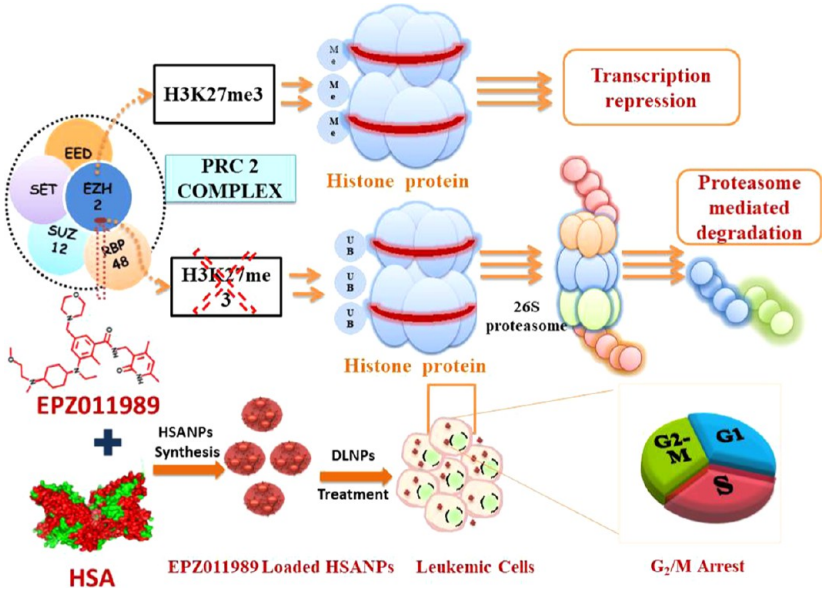

PRC2, controls the equilibrium between self-renewal and differentiation in hematopoiesis. It deposits the histone mark H3K27me3, which promotes transcriptional repression and cell cycle regulation.[15] During epigenetic gene silencing, PRC2 trimethylates histone H3 at lysine 27 and recruits members of PRC1 having E3 ligase activity for monoubiquitination of histone H2A at lysine 119, which results in transcriptional repression of tumor suppressor genes. The overexpression of EZH2 is already linked with the development of acute myeloid leukemia, which makes EZH2 a favorite target in epigenetic cancer therapeutic.[16,17] Pharmacological targeting of EZH2 could be a newer therapy in cancer, but the least knowledge of the underlying mechanisms of EZH2 regulation and posttranslational modifications make this approach challenging.[18] The attachment of multiple ubiquitin molecules covalently and associated 26S proteasome-directed degradation of the proteins is one of the key regulatory processes.[19]

The transcription factor c-Myb plays a crucial role in the hematopoiesis process,[20] and its overexpression is implicated in the development of leukemia. Thus, the mechanism regulating c-Myb expression could emerge as a potential therapeutic strategy for controlling AML.[21]

The present standard therapeutic modalities of AML, including chemotherapy, bone marrow/stem cell transplantation, targeted therapy, and radiation therapy, suffer from nonspecific targeting, limited efficacy, the complexity of the procedures, less bioavailability of the chemotherapeutic drug, and adverse side effects.[22]

Targeted nanomedicines are recently developing into a master class approach to overcome such therapeutic limitations. Also, the epigenetic modifications are reversible in function, which provides us a window to use targeted nanomedicine using specific inhibitors of histone-modifying proteins or proteins driving and maintaining DNA methylation in the cell.[22] Therefore, targeting EZH2 is the most appropriate novel approach that can be considered for a new generation of AML therapy.

The drug EPZ011989 (*N*((4,6-dimethyl-2-oxo-1,2-dihydropyridin-3-yl)methyl)3-(ethyl ((trans)4-(2-methoxyethyl)-(methyl)amino)cyclohexyl)-amino)-2-methyl-5-(3-morpholinoprop-1-yn-1-yl) benzamide is a potential inhibitor of EZH2, with considerable inhibitory potential compared to EPZ 6438, EPZ005687, and GSK-126 but is associated with poor solubility and less bioavailability.[23] The protein nanoparticle-based nanoformulation of EPZ011989 can overcome these limitations and improve its efficacy with enhanced regulation of PcG in AML. The abundant plasma protein human serum albumin (HSA) transports different key biomolecules across different visceral sites inside the human body. HSA-based nanocarriers demonstrated high drug loading and binding capability,[24] excellent distribution, non-immunogenicity, and biodegradability, which make it a material of choice for using as a matrix for drug encapsulation and therapeutic use.[25,26] In the previous reports, the HSANPs have been used for delivery of doxorubicin,[27] co-delivery of pirarubicin with paclitaxel,[28] and delivery of noscapine with enhanced drug efficacy.[29]

In present work, EPZ011989 is being formulated in HSANPs for the first time for effective epigenetic suppression that could lead to successful AML therapy. Moreover, EPZ011989-loaded HSANPs with important physicochemical characteristics, controlled drug release, enhanced AML cell uptake, and G2/M phase cell cycle arrest were positively associated with the enhanced inhibition of EZH2 expression and antileukemic activity in the U937 AML cell line. This nanoformulation-mediated suppression of the leukemic cell proliferation, induction of apoptosis, and mitochondrial damage leading to overexpression of caspase 3 are suspected as the underlying mechanisms of the anticancerous action. The detailed molecular investigation showed that targeting of EZH2 expression was associated with increased ubiquitination, which is reversed upon cellular proteasomal inhibition (Scheme 1). Moreover, the role of another target, c-Myb, is investigated as a direct modulator of EZH2, which binds to a specific promoter region and also interacts at the protein level, and siRNA-based silencing of c-Myb reduces these interactions. EPZ011989-loaded HSANPs with negligible nonspecific systemic toxicity and considerable circulation time demonstrated superior anti-AML efficacy on the in vivo AML xenograft model. Thus, this strategic nanostructure

DOI: 10.1021/acs.molpharmaceut.9b01071
Mol. Pharmaceutics XXXX, XXX, XXX−XXX

exhibiting anticancerous activity via epigenetic inhibition may potentially contribute to the development of novel epigenetic regulation-based antileukemic therapeutics.

2. EXPERIMENTAL SECTION

2.1. Materials. Human serum albumin (HSA, A2153, Reliance Life Sciences), glutaraldehyde 25% w/v solution (RM5927), MTT dye (TC191), PI (TC252), streptomycin−penicillin solution (A018), RPMI 1640 (AL162S), fetal bovine serum (FBS; RM9955), and trypsin-EDTA were purchased from Himedia; dialysis membrane 12 kD (D6191) and ethanol were purchased from Merck (1.00983.0511); and mannitol (M4125) was purchased from Sigma-Aldrich. The Annexin Cy3/CFDU kit (Sigma), JC-1 cyanine dyes (Abcam), and DAPI (Himedia) were used. All antibodies were purchased from either Cell Signaling Technology (Danvers, MA) or Santa Cruz Biotechnology (Santa Cruz, CA).

2.2. EPZ011989-Loaded HSANP Preparation. The placebo HSA nanoparticles were prepared following the desolvation method. Briefly, ethanol (90%) was added dropwise under constant magnetic stirring conditions in the homogenous solution of HSA at pH 8.2. The EPZ011989-loaded HSANPs were prepared by dropwise addition of the EPZ011989 into the 2% homogenous HSA solution in the mass ratio of 1:6. Both placebo HSANP and EPZ011989-loaded HSANP solutions were added with 8% glutaraldehyde solution (1.175 μL/mg of protein) and left for magnetic stirring for 24 h. Following three consecutive washing cycles with Milli-Q water using centrifugation at 35 000*g*, the purified placebo HSANP and EPZ011989-loaded nanoparticles were recovered and lyophilized.

2.3. EPZ011989 Loading Efficiency and Encapsulation Efficiency. The effective loading of EPZ011989 was estimated following the indirect method by accurately measuring the drug remained in the supernatant of the reaction mixture. The high-performance liquid chromatography system (HPLC, Waters technology) was used for the measurement using a photodiode array detector. The autosampler was used to inject 20 μL of the sample in the C18 column (water Spherisorb, 250 × 4.6 mm^2, 5 μm). The acetonitrile/distilled water (95/5% v/v) solution was used as a mobile phase, with a flow rate of 1.5 mL/min and a detection wavelength of 303 nm. The retention time of EPZ011989 was 14.32 ± 0.38 min observed based on the integrated peak area from the calibration curve of EPZ011989 (R^2 = 0.992) at concentrations varying from 0.2 to 0.6 mg/mL. The drug loading and drug entrapment efficiency were calculated using the following formula

$$\text{drug EE (\%)} = \frac{\text{amount of the drug added} - \text{amount of the drug in the supernatant}}{\text{amount of drug added}} \times 100$$

$$\text{drug loading (\%)} = \frac{\text{amount of the drug added} - \text{amount of the drug in the supernatant}}{\text{weight of nanoparticles}} \times 100$$

2.4. Characterization of HSANPs and EPZ011989-loaded HSANPs. A particle size analyzer (Malvern. Inc.) was used to measure the hydrodynamic diameter and the ζ-potential of the HSANPs and EPZ011989-loaded HSANPs. Transmission electron microscopy (TEM) images were obtained on JSM 2100 operated at 120 kV. Field emission scanning electron microscopy (FESEM) samples were prepared by drop-casting them on a silicon wafer, air-dried, and sputtered with a thin layer of gold before imaging. The atomic force microscopy (AFM) imaging was performed on Bruker Multimode 8 using a silicon nitrite tip in tapping mode on the diluted sample on the silicon wafer. The circular dichroism (CD) spectra were recorded on the JASCO J-1500 spectrophotometer (Easton, MD) using demountable cells (0.1 mm path length, Hellma). The UV−vis absorbance spectra for studying the EPZ011989 interaction with HSA were collected using a UV−vis spectrophotometer. The Fourier transform infrared (FTIR) spectra were recorded on a Cary Agilent 660 IR spectrophotometer, with 256 scans 4 cm^{-1} resolution in the range of 400−4000 cm^{-1}. X-ray diffractograms (XRD) of the nanoformulation were recorded on a Bruker powder D8 X-ray diffractometer with a scan rate of 0.2 scans per minute at 2θ values of 2−80°. Microtiter plate reader BioTek Synergy 2, Finland, was used for recording the absorbance and steady-state fluorescence spectra of HSA, HSANP, and EPZ011989-loaded HSANPs. In silico docking studies were performed using iGEMDOCKv2.1.[30] The PDB crystal structure of HSA (PDB ID: 1AO6) and the ligand three-dimensional (3D) structures were prepared using ChemDraw Ultra 14.0 software (Cambridge Soft, Cambridge, MA). Differential scanning calorimetry (DSC, PerkinElmer, DCS8000) was used for estimating the stability of the nanoformulation.

2.5. In Vitro Drug Release, Nanoformulation Solubility, and Stability Analysis. The in vitro drug (EPZ011989) release studies were performed using HSA as a receiver phase in 20% ethanolic solution of phosphate buffer saline (20 mL, phosphate-buffered solution (PBS), pH 7.4) and using the dialysis membrane (MWCO 12 kDa) method for 1 mg of the nanoformulation taking in triplicates at 37 °C under magnetic stirring at 150 rpm. HSA was used in the receiver phase, and the free drug and nanoformulation with ethanol solvent were used in the donor phase. Then, 1 mL of the sink buffer aliquot at a different time point was replenished with equivalent fresh buffer. The diluted solution of these aliquots was analyzed using HPLC. The drug solubility study was performed in PBS, considering 0.5 mg/mL EPZ011989 and an equivalent amount of EPZ011989-loaded HSANPs, respectively. The UV−vis spectrum of the aliquot was collected intermittently. The nanoformulation stability study was performed mimicking the different physiological conditions of Dulbecco's modified Eagle's medium (DMEM) and DMEM + 10% FBS for EPZ011989-loaded HSANPs and placebo HSANPs, and the variation in particle diameter and ζ-potential was analyzed using a particle size analyzer.

2.6. Cell Culture. U937 (myeloid lymphocytic cells) and HL60 (promyeloblast) from human origin acute myeloid leukemia cells and HEK293T were procured from the Curator, cell repository, National Center of Cell Science, Pune, India, and maintained in the cell culture medium RPMI 1640 supplemented with 10% FBS and 1% antibiotic solution at 37 °C under 5% CO_2 in an incubator.

2.7. Cell Cytotoxicity, Cellular Uptake, Cell Cycle Arrest, Apoptosis, and Mitochondrial Transmembrane Potential ($\Delta\Psi_m$) Studies. The cellular toxicity of the prepared nanoformulation, drug, and placebo nanoparticles was assayed on U937, HL60, and HEK293T cells (1 × 10^4 cells/well) at varying treatment concentrations, and the viability was measured using the MTT reagent, by taking absorbance at 570 nm. The rhodamine-B-tagged placebo HSANPs and

DOI: 10.1021/acs.molpharmaceut.9b01071
Mol. Pharmaceutics XXXX, XXX, XXX−XXX

EPZ011989-loaded HSANPs were exposed to U937 cells (5×10^3 cells) at a concentration of 25 μg/mL for 4 h. The cells were collected, mounted on a slide, and imaged under a confocal laser scanning microscope (LSM880, Zeiss Ltd). For DNA content-based cell cycle analysis, the U937 cells were first synchronized before treatment. To synchronize the cell cultures, U937 cells were seeded in the growth medium with 10% FBS overnight. Following washing with PBS, these cells were cultured in serum-free medium.[31] After serum starvation for 24−48 h, these cells were treated with EPZ011989-loaded HSANPs, placebo HSANPs, and EPZ011989 for the next 72 h in complete medium with 10% FBS, which is proceeded with the cell cycle measurement using multiple assays. These cells were fixed with ethanol, treated with RNAse-A, stained with propidium iodide (PI, 10 μg/mL), acquired on a flow cytometry system (BD FACS, Aria III) for cell cycle, analyzed, and plotted on Flowjo software (v10). Further, U937 cells were treated and separately processed for JC-1 (10 μg/mL) staining and directly processed for FACS acquisition. The U937 cells (1×10^5) were treated with EPZ011989-loaded HSANPs, placebo HSANPs, and EPZ011989 for 72 h and processed for Annexin V-Cy3 and 6-carboxyfluorescein (6-CFDA) (APOAC, apoptosis detection kit, Sigma-Aldrich) staining following the manufacturer protocol.

2.8. Bromodeoxyuridine (BrdU) Incorporation-Based Active S phase Measurement. The U937 cells (1×10^6) were treated with placebo HSANPs, EPZ011989, and EPZ011989-loaded HSANPs for 72 h and exposed to bromodeoxyuridine (BrdU, 10 μM) for 2 additional hours of incubation following an earlier reported protocol. The cells were fixed using 1 mL of absolute ethanol (4 °C for 1 h), collected using centrifugation (4000 rpm, 4 °C, 10 min), and incubated with 0.5 mL, 2 N HCl/0.5% Triton X-100 for 30 min at room temperature. The cells were neutralized with 1 mL of 100 mM tetraborate buffer, washed with PBS/1% BSA, and incubated with anti-BrdU primary antibody (1:500, cat no. 317902 BioLegends Ltd.) for 1 h at RT. The cells were washed two times with a washing solution (PBS/1% BSA/0.3% Tween-20). The cells were incubated with the FITC-tagged IgG secondary antibody for 1 h. The collected cells were resuspended in the buffer containing 10 μg/mL RNAse-A and 20 μg/mL PI, incubated for 30 min, and processed for FACS acquisition.

2.9. Colony Formation Assay. The two-layer technique was used for the colony formation assay in which the first layer consists of 1% agar base layer and the second layer contains U937 cells in 0.5% agar. Briefly, equal volumes of the base agar containing 1% agar along with 2× RPMI containing 20% FBS were mixed to obtain 0.5% agar and 1× RPMI with 10% FBS. The cells were treated with placebo HSANPs, EPZ011989, and EPZ011989-loaded HSANPs for 72 h, and 1000 cells were mixed with 1.5 mL of 0.5% agar and added over the base agar layer in 6-well plates. These plates were incubated for 14 days at 37 °C and 5% CO_2, and formed colonies were intermittently observed using an inverted microscope and stained with 0.1% crystal violet solution to visualize the generated colonies. The colony forming efficiency (CE) was calculated by the number of colonies in the treated sample and divided by the number of cells added to each plate.

2.10. Real-Time Quantitative PCR (qPCR) Analyses. Total RNA from U937 cells (1×10^7) treated with placebo HSANPs, EPZ011989, and EPZ011989-loaded HSANPs was isolated using the PureLink RNA mini isolation kit (12183018A, Applied Biosystem). The cDNA was prepared with reverse transcription (RT-PCR) using a high-capacity cDNA reverse transcription kit (cat-4368813, Applied Biosystem) following the kit protocol. Then, 100 ng of the cDNA template and 300 ng of the primers were used in 20 μL of the reaction volume for real-time PCR cycles. The primer sequence for specific gene targets EZH2 and BMI-1 is provided in Supporting Information Table S2. The qPCR reaction was performed on a thermal cycler (Quant Studio 3, real-time PCR instrument, A28132, Applied Biosystems) with an initial step at 50 °C for 2 min followed by 40 cycles of 95 °C for 15 s and then 60 °C for 1 min. The Ct, ΔΔCt, and the fold change for each gene were calculated based on the relative threshold values against the indigenous GAPDH control. All of the experiments were performed in independent triplicate, statistically analyzed, and represented.

2.11. Western Blot and Immunoprecipitation Assay. The U937 cells were treated with placebo HSANPs, EPZ011989, and EPZ011989-loaded HSANPs for 72 h, and whole-cell protein lysates were prepared in radioimmunoprecipitation (RIPA) buffer. Following Bradford quantitation, 25 μg/mL protein was separated by sodium dodecyl sulfate-polyacrylamide gel electrophoresis (SDS-PAGE), transferred to poly(vinylidene fluoride) (PVDF) membranes, blocked with 5% BSA, and probed with respective primary antibodies anti-BMI-1 (SC-390443), anti-ENX1 (SC-166609), anti-caspase 3 (SC-56053), anti-c-Myb (sc-74512), anti-β-actin (SC-69879), and anti-ubiquitin (SC-8017) procured from Santacruz Biotechnology (SCBT) and anti-histone-3 (14269S), trimethyl-histone H3 (Lys27) (9733S), and ubiquity-histone H2A (Lys119) (8240S) procured from Cell Signaling Technology. The secondary anti-mouse IgG-HRP antibody (SC-516102) and anti-rabbit IgG-HRP (SC-71675) were purchased from SCBT. The presence of the protein on the blot was visualized using an ECL substrate (BIO-RAD) and followed by detection through image J lab software and a ChemiDoc XRS+ imaging system. For investigating the role of the proteasome pathway, the cells were pretreated with MG132 (1 μM) for 4 h, following exposure to placebo HSANPs, EPZ011989-loaded HSANPs, and EPZ011989 for 72 h. The cell lysate was isolated and examined following a similar procedure.

The cell lysates (300 μg) from differently treated groups were incubated with anti-IgG, anti-BMI-1, anti-EZH2, and anti-c-Myb primary antibodies for 1 h. The lysate was incubated with precleared A/G beads (sc-2004, SCBT) on a rotary shaker at 4 °C overnight. The precipitated A/G beads after centrifugation were washed two times with PBS and immunoblotted following the above procedure using primary antibodies anti-BMI-1, anti-EZH2, anti-c-Myb, and anti-ubiquitin.

2.12. siRNA-Based Silencing of c-Myb. U937 cells were seeded in 2 mL of antibiotic-free media supplemented with 10% FBS and incubated at 37 °C in a CO_2 incubator for 18−24 h. The c-Myb siRNA (sc-29855) (2−8 μL) in 100 μL of transfection media (sc-36868) and 2−8 μL of transfection reagents (sc-29528) in 100 μL of transfection media (sc-36868) were mixed and left for 45 min at room temperature. The common pool of three siRNA duplexes (sc-29855A) with the sequence sense- GGAACAGAAUGGAACAGAUtt, antisense-AUCUGUUCCAUUCUGUUCCtt; (sc-29855B) sense-GAACUCCUACACCAUUCAAtt, antisense-UUGAAUGGUGUAGGAGUUCtt; and (sc-29855C) sense-GUACUCCAGUAUUUCACUUtt, antisense- AAGUGAAAUACUGGAGUACtt were used. This mixture was overlaid onto the washed cells and incubated for 48 h with the addition of fresh growth media. The whole-cell protein lysates were prepared

DOI: 10.1021/acs.molpharmaceut.9b01071
Mol. Pharmaceutics XXXX, XXX, XXX−XXX

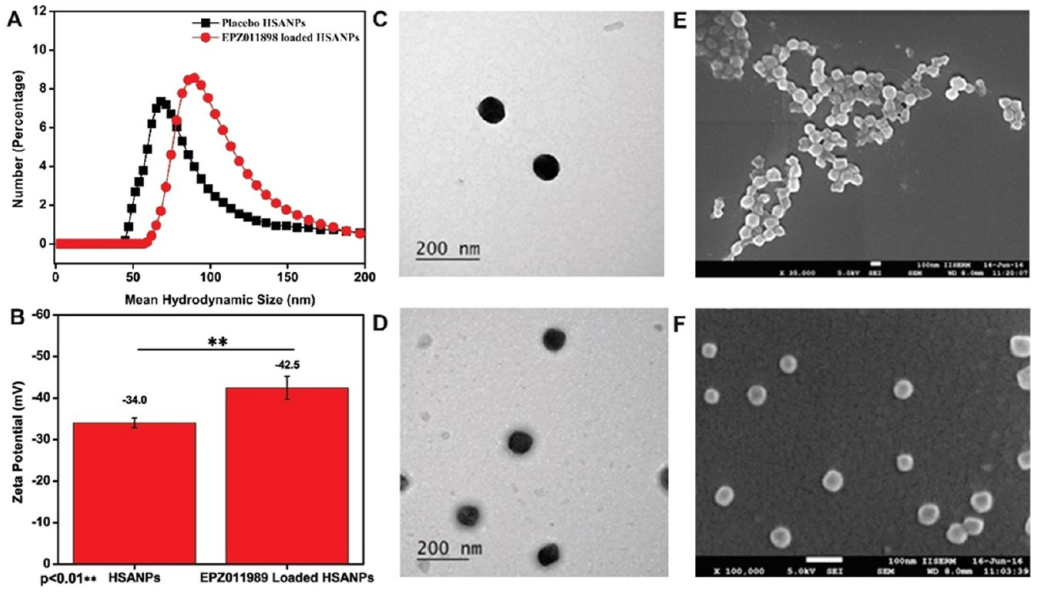

Figure 1. Mean hydrodynamic diameter distribution of placebo HSANPs and EPZ011989-loaded HSANPs centered at 68 ± 17 and 87 ± 8 nm, respectively (A); the ζ-potential values of placebo HSANPs and EPZ011989-loaded HSANPs of −26.5 ± 10 and −33.4 ± 12 mV are represented in the histogram. The Student *t*-test at the $^{**}P < 0.01$ ($n = 3$) significance level performed for statistical comparison (B); TEM micrographs of placebo HSANPs (C) and EPZ011989-loaded HSANPs (D); and FESEM images of placebo HSANPs (E) and EPZ011989-loaded HSANPs (F).

using radioimmunoprecipitation (RIPA) buffer and examined by immunoblotting following the western blotting protocol. The primary antibodies anti-ENX1 (sc-166609) and anti-c-Myb (sc-74512) and the secondary anti-mouse IgG-HRP antibody (sc-516102) were used for detection.

2.13. Chromatin Immunoprecipitation (ChIP) Assay. The U937 cells (1×10^7) following treatment with the drug and DLNPs for 72 h along with the untreated control were processed for the ChIP assay following the standard protocol. Briefly, the cells were fixed using a formaldehyde solution (11%) and lysed using sonication (amplitude) for 10 min at 4 °C to obtain sheared DNA fragments. The fragments were incubated and precipitated with the c-Myb antibody (CST), after which DNA−protein immunocomplexes were collected, using protein A/G-agarose beads (SCBT), and treated with RNase-A (Sigma) and proteinase K (Sigma); primers were used for the promoter region of the EZH2 gene (Supporting Information Table S2). The enrichment of c-Myb motif binding at or around EZH2 could be reliably detected and quantified by the ChIP-real-time PCR assay, and the PCR products were run on 2% agarose gel in 1× TBE buffer.

2.14. In Vivo and ex Vivo Biodistribution of Nanoparticles. In vivo whole-body imaging experiments on 4−6-week-old male BALB/c mice were performed after due ethical clearance from the Institutional Animal Ethics Committee. The BALB/c mice were injected via tail vein with 100 μL of 5 mg/mL EPZ011989-loaded HSANPs, and the photoluminescence (IVIS spectrum) of indocyanine green (ICG) was observed till 4 h with a time duration of 30 min for acquisition. EPZ011989-loaded HSANPs were incubated with the ICG (indocyanine green) staining dye for 24 h in shaking conditions at room temperature, followed by dialysis for 3 days to remove the unbound dye. The EPZ011989-loaded HSANPs were collected from the dialysis membrane and used for the experimental studies. The animals were dissected and the kidney, spleen, liver, brain, and heart were collected and imaged separately. The histopathological assessment was performed by staining the organ tissue section obtained from the mice with prolonged administration of the EPZ011989-loaded HSANPs and EPZ011989.

2.15. In Vivo Efficacy Studies in the Mouse Xenograft Model. The 4-week-old female nude mice were used, and all studies were conducted following guidelines of the Institutional Animal Ethical Committee (IAEC) of Indian Institutes of Science Education and Research, Mohali. The acute myeloid leukemia xenograft model was developed by first treating the animals with 20 mg/kg busulfan (ip administration) for 24 h followed by injection of leukemic cells (iv). Before administration, U937 cells were washed twice in phosphate-buffered saline (PBS) and cleared of aggregates followed by intravenous administration of 2 million AML cells/200 μL of PBS per mouse. These animals, upon completion of 4 weeks bearing xenografts, were divided into the following groups: control group (without therapy), placebo HSANP group, EPZ011989 (EPZ) administration group, and EPZ011989-loaded HSANP group. These formulations were injected intraperitoneally (ip) including four cycles of 5 consecutive days of injection with 1 day rest between cycles. The immunophenotyping of $CD45^+$ and $CD11b^+$ (PerCP/Cy5.5, 304027 & $CD11b^+$APC/Cy7, 10125 were purchased from Biolegends Ltd.) positive cells in mouse peripheral blood and bone marrow was quantitated using a flow cytometer. For confirming leukemic engraftment, the mice were humanely sacrificed and bone marrow and spleen were dissected, crushed in PBS, and made into single-cell suspensions for analysis by a flow cytometer. The protein levels of EZH2, c-Myb, and caspase 3 isolated from the bone marrow cells and spleen tissue of differently treated groups were analyzed using western blotting. The whole spleen and histological sections of spleen from treated mice were prepared and stained with hematoxylin and eosin (HE) by following the standard protocol.

2.16. Statistical Analysis. All data were analyzed and quantitated and drawn in OriginLabv8.5. The nonlinear and linear fittings, the statistical comparison using Student's *t*-test, and one-way and two-way analysis of variance (ANOVA) were

DOI: 10.1021/acs.molpharmaceut.9b01071
Mol. Pharmaceutics XXXX, XXX, XXX−XXX

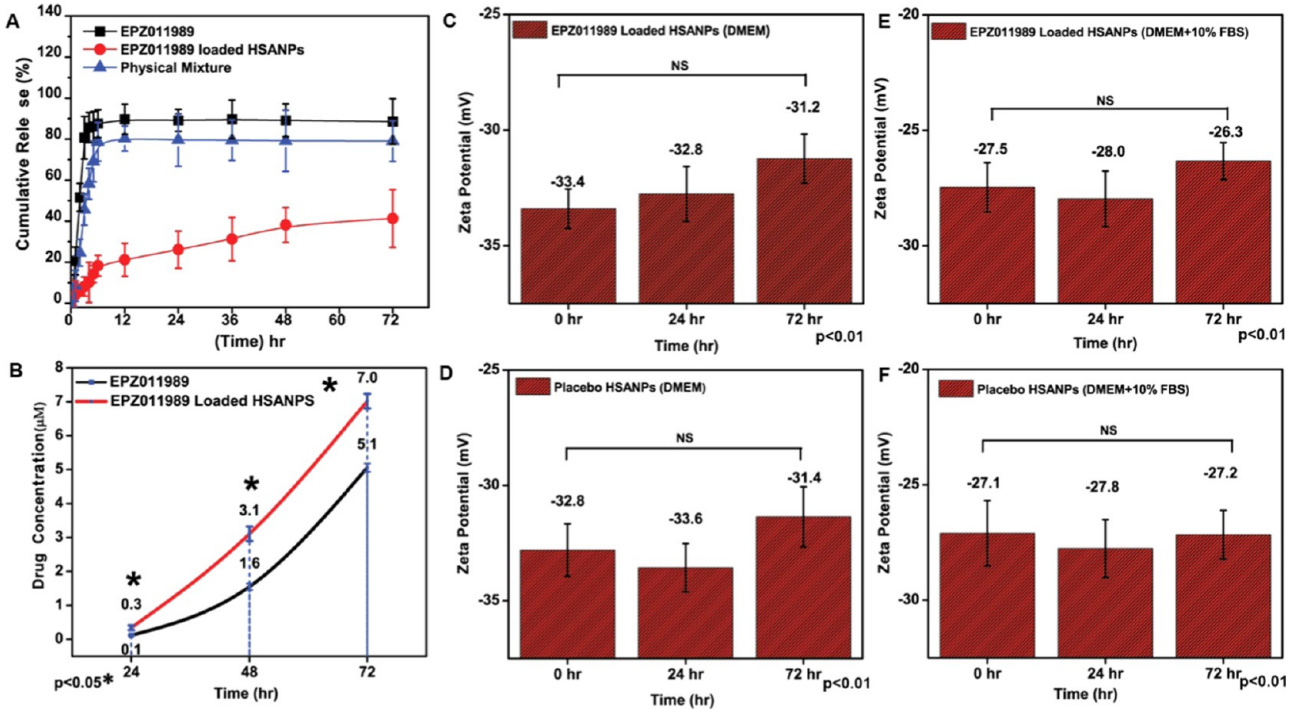

Figure 2. Percentage cumulative drug release profiles of EPZ011989, EPZ011989-loaded HSANPs, and physical mixture (A); solubility profiles of EPZ011989 and EPZ011989-loaded HSANPs (B); ζ-potential values of the EPZ011989-loaded HSANPs (C and E) and HSANPs (D and F) in DMEM and DMEM + 10% FBS, respectively, at different time points showing the stability of nanoformulation. The Student *t*-test at $^{*}P < 0.05$ and one-way ANOVA with the Tukey test at the $^{**}P < 0.01$ ($n = 3$) significance level are performed for statistical comparison.

performed following Tukey's test for mean comparison among the groups at the *P*-values of *≤0.05, **≤0.01, and ***≤0.001.

3. RESULTS

3.1. Preparation and Characterization of EPZ011989-Encapsulated HSANPs. In this work, placebo HSANPs and EPZ011989-loaded HSANPs were prepared by the desolvation method following standard protocols.[32] The mean hydrodynamic diameters were found to be around 68 ± 17 nm and 87 ± 8 nm with a monodispersed solution phase indicated by the polydispersity index (PDI) < 0.2 for HSANPs and EPZ011989-loaded HSANPs, respectively, measured via dynamic light scattering (DLS) (Figure 1A). The ζ-potentials of placebo HSANPs and EPZ011989-loaded HSANPs were −26.53 ± 12 and −33.43 ± 10 mV, respectively (Figure 1B). The detailed morphological features of the placebo HSANPs and EPZ011989-loaded HSANPs were obtained by field emission scanning electron microscopy (FESEM), transmission electron microscopy (TEM), and atomic force microscopy (AFM). TEM (Figure 1C,D), FESEM (Figure 1E,F), and AFM (Supporting Information Figure S1A,B) images revealed the uniform spherical morphology of both placebo HSANPs and EPZ011989-loaded HSANPs with a mean diameter of ∼100 nm. The calculated drug loading and drug entrapment efficiency estimated were 14.23% ± 21 and 95% ± 13, respectively. To determine the interactions and the chemical modifications during the preparation process, Fourier transformation infrared (FTIR) analysis was conducted. Characteristic sharp peaks of EPZ011989 were observed at 1116 and 1635 cm^{-1}. Other significant peaks including 3301 and 3057 cm^{-1} are consistent with the HSA and HSA with EPZ011989 (physical mixture). The shifting of the amide I peak toward a higher wave number observed at 1660 cm^{-1} in EPZ011989-loaded HSA nanoparticles indicated EPZ011989 interaction with HSA during the encapsulation process (Supporting Information Figure S2A). EPZ011989 powder displayed crystalline characteristic diffraction peaks at a 2θ value of 18.6 in X-ray diffraction (XRD) consistently appearing in a physical mixture of EPZ011989 and HSA nanoparticles, although HSA, placebo HSANPs, and EPZ011989-loaded HSANPs showed almost amorphous characteristics, supporting complete entrapment of EPZ011989 inside nanoparticles (Supporting Information Figure S2B). The circular dichroism spectroscopy results showed a transition in the secondary structure of the HSA during nanoparticle preparation from α-helix to β-sheet and random coils (Supporting Information Figure S2C), as HSA natively exists in the majority of α-helix (222 and 208 nm) conformation turns in to β-sheet (216 nm) and random coils (217 nm) indicating the degree of protein aggregation and denaturation. The CD data gave information about the mechanism of nanoparticle preparation via the desolvation method. On addition of the desolvating agent, EPZ011989 with HSA forms nanoaggregates, later stabilized by glutaraldehyde as a cross-linking agent. This facilitates improved drug release, as evident in the in vitro drug release profile.

Moreover, the differential scanning calorimetric (DSC) thermogram further supports the XRD results as EPZ011989 showed crystalline peaks in the DSC melting curve at 96, 223, 231, 240, 247, and 255 °C (Supporting Information Figure S3). The melting curve of physical mixture displayed two peaks at 76 and 208 °C, whereas no peaks were observed in EPZ011989-loaded HSANPs. Interestingly, to confirm EPZ011989 and HSA interactions, UV spectral absorbance and steady-state tryptophan fluorescence emission intensity have been recorded. Mixing of 5 μM HSA with varying concentrations of 15, 20, 25, and 50 μM of EPZ011989 has shown absorbance λ_{max} within

DOI: 10.1021/acs.molpharmaceut.9b01071
Mol. Pharmaceutics XXXX, XXX, XXX−XXX

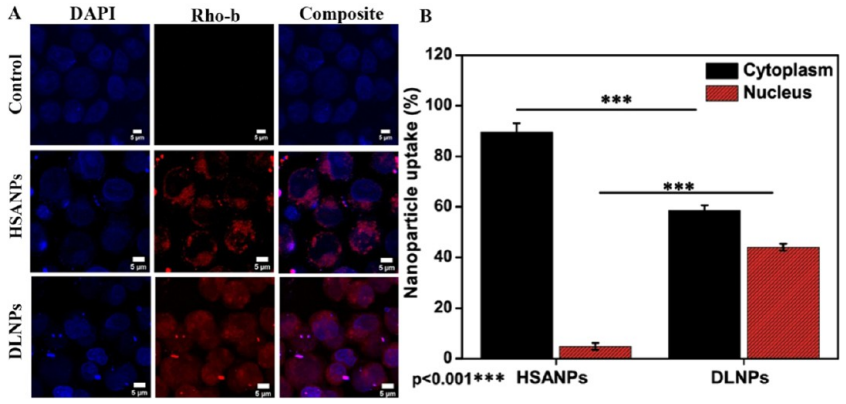

Figure 3. Cellular uptake of HSANPs (placebo HSANPs) and DLNPs (EPZ011989-loaded HSANPs) tagged with rhodamine B (red) in U937 cells & DAPI stained nucleus (blue), scale bar = 5 μm (A), and their quantitative analysis for (%) uptake in cytoplasm and nucleus (B). The Student *t*-test at the ***$P < 0.001$ ($n = 3$) significance level is performed for statistical comparison.

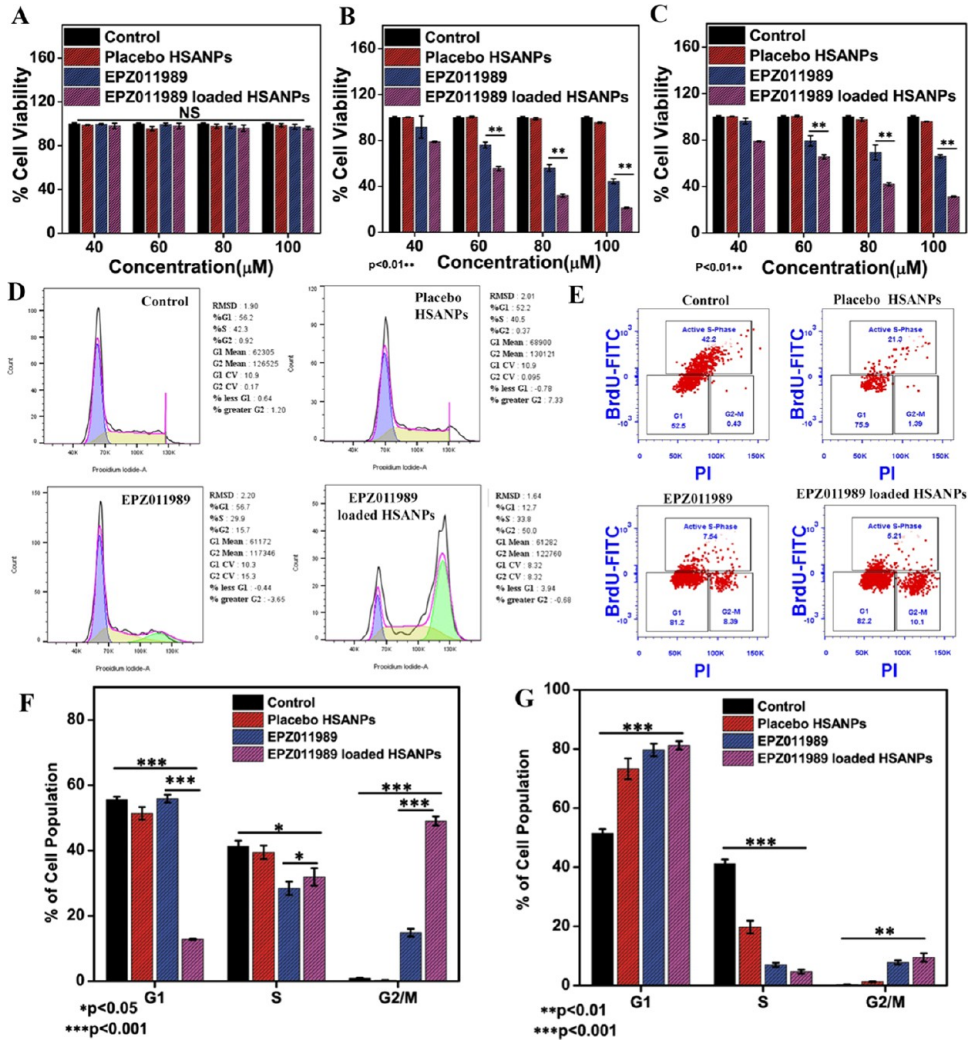

Figure 4. In vitro cell viability measurement following treatment with control, placebo HSANPs, EPZ011989, and EPZ011989-loaded HSANPs on 293T (A), HL60 (B), and U937 cell lines (C). The FACS-based cell cycle analysis of the treated U937 cell population (D). The FACS-based measurement of BrdU incorporation vs DNA content (PI staining) of treated U937 cells (E). The quantification of percentage cell population in different cell cycle stages G1, S, and G2/M is represented as a bar diagram for PI-stained (F) and BrdU and PI dual stained (G) populations. The statistical comparison was performed using one-way ANOVA with Tukey's test at *$P < 0.05$; **$P < 0.01$; and ***$P < 0.001$ ($n = 3$) significance levels.

the 230 and 300 nm range, primarily indicating the absence of any physical covalent interactions between HSA and EPZ011989 (Supporting Information Figure S4A). However, the quenching of steady-state tryptophan fluorescence maxima of 5 μM HSA positively correlated with the increasing concentration of EPZ011989, showing the noncovalent

DOI: 10.1021/acs.molpharmaceut.9b01071
Mol. Pharmaceutics XXXX, XXX, XXX−XXX

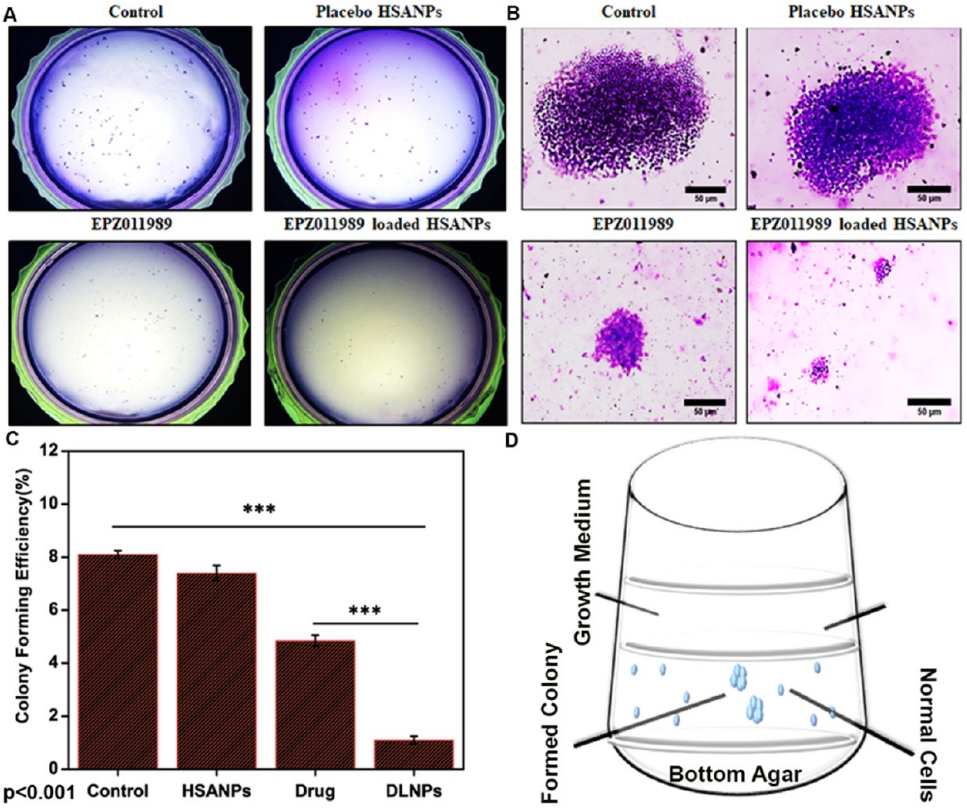

Figure 5. Colony formation assay for U937 cells colonies treated with placebo HSANPs, EPZ011989, and EPZ011989-loaded HSANPs and stained with crystal violet and images of the whole plate (A); the enlarged view of a single colony at higher magnification (B). The quantitative colony forming capacity of the differently treated U937 cells is represented as a histogram. All of the values are compared using one-way ANOVA with the Tukey test at ***$P < 0.001$ significance level (C) and the schematic illustrating the colony formation assay setup (D).

interactions of HSA with EPZ011989 in an aqueous environment (Supporting Information Figure S4B). In silico, molecular docking analysis was performed with iGEMDOCK, which shows molecular interactions (Supporting Information Figure S4C) and suggests that several amino acid residues played an essential role in the binding of EPZ011989 with HSA and EZH2 (Supporting Information Table S1).

3.2. EPZ011989 Release Pattern, Solubility, and Stability Analysis. This conformational characteristic of HSA-based nanocarriers facilitates improved drug release as represented by the in vitro drug release profile (Figure 2A) referenced to the EPZ011989 standard curve obtained via HPLC showing retention time at 303 nm (Supporting Information Figure S5). The free drug EPZ011989 showed burst release of ∼85% drug in initial 4 h, and a similar pattern is recorded in the physical mixture of EPZ011989 and HSANPs (wt %) showing 80% drug released in initial 12 h. The EPZ011989-loaded HSANPs provided an initial burst phase followed by the controlled release with only ∼20% drug released in the initial 12 h and total 41% in 72 h of the experiment. The solubility profiles of free EPZ011989 and EPZ011989-loaded HSANPs in 1× PBS show a significant increase in the solubility till 72 h (Figure 2B). The result shows that the major solubility problem of EPZ011989 can be overcome after encapsulation with HSANPs, which increase its solubility. The stability study shows the compatibility of the EPZ011989-loaded HSANPs in various physiological fluid conditions as a function of particle diameter (Supporting Information Figure S6A−D) and ζ-potential (Figure 2C−F) in DMEM and DMEM + 10% FBS.

3.3. Cellular Uptake and Cytotoxicity of the Nanoformulation on AML Cells. The acute myeloid leukemia (AML) cells U937 and HL60 of the human origin were used for assessing in vitro anti-AML therapeutic efficacy of EPZ011989 nanoformulation. Both cell lines are EZH2-positive with 87% (U937 cells) and 60% (HL60 cells) overexpression of EZH2, which validates their use as an in vitro model in our work and is also demonstrated in previous reports.[33,34] The placebo HSANPs and EPZ011989-loaded HSANPs were firmly tagged with fluorescent dye rhodamine B and exposed to U937 cells for a variable period. The imaging done by confocal laser scanning microscopy (CLSM) of these cells displayed nuclear localization of EPZ011989-loaded HSANPs in U937 cells, whereas the rhodamine B-tagged placebo HSANPs accumulated in the cytoplasm. These observations confirmed that EPZ011989-encapsulated HSANPs direct their accumulation in the nucleus in the leukemic cell line (U937) and placebo HSANPs accumulate into the cytoplasm. The colocalization of the blue fluorescence of nuclear material stained with DAPI and red fluorescence of DLNPs accumulated clearly show the potential of DLNPs to localize into the cell nucleus (Figure 3A,B). The color-intensity-based histogram for the whole cell and nucleus region is represented for HSANPs and DLNPs, where HSANPs show negligible fluorescence in the nucleus and DLNPs show the nuclear uptake (Supporting Information Figure S7).

EPZ011989, as an inhibitor of EZH2, shows different IC_{50} values depending upon the cell type and origin and treatment schedule.[23,35] Inhibition of the cellular growth and proliferation was evaluated in time and concentration-dependent manner, ranging from 40 to 100 μM concentration of drug and equivalent

DOI: 10.1021/acs.molpharmaceut.9b01071
Mol. Pharmaceutics XXXX, XXX, XXX−XXX

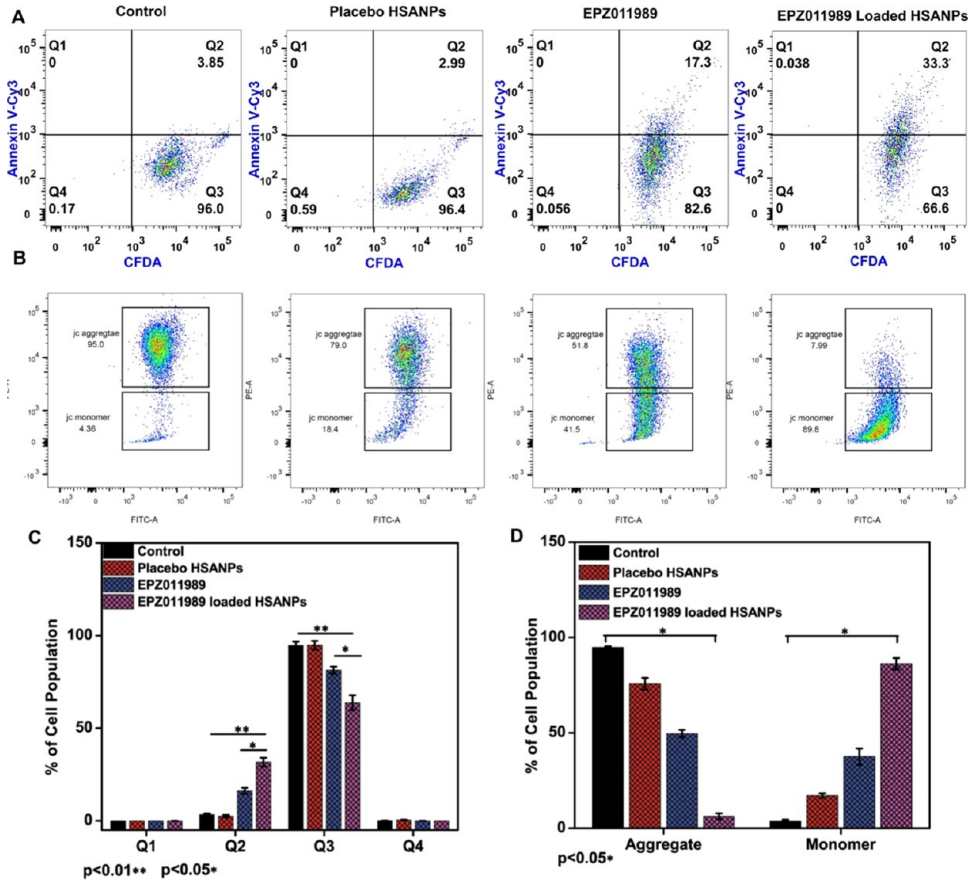

Figure 6. Apoptosis activity of the nanoformulation determined by Annexin V-Cy3 and 6-carboxyfluorescein (CFDA) dual staining followed by flow cytometric analysis of the U937 cells treated with apoptotic and necrotic EPZ011989, placebo HSANPs, and EPZ011989-loaded HSANPs, respectively (A). The mitochondrial membrane depolarization following treatment with EPZ011989, placebo HSANPs, and EPZ011989-loaded HSANPs was measured using FACS (B). The U937 cell population undergoing apoptosis is quantitatively represented in a histogram (C). The treated population shifting from aggregates JC-1 (red) to monomers (less red) upon mitochondrial damage is quantitatively described (D). All of the values are expressed as mean ± standard deviation ($n = 3$) and compared using one-way ANOVA with the Tukey test at $^*P < 0.05$ and $^{**}P < 0.01$ significance levels for statistical comparison.

loading in HSANPs in 293T, U937, and HL60 cell lines. The noncancerous 293T cells showed no significant inhibition and cytotoxicity (Figure 4A), whereas similar doses of EPZ011989 and EPZ011989-loaded HSANPs exhibited significant cytotoxicity in U937 and HL60 (Figure 4B,C). The results indicated that the selective targeting of the EZH2-positive cells is more prone to cellular death as the similar optimal dose of either drug or nanoformulation does not have any effect on the viability of normal cells. The dose−response curve of the EPZ011989 and EPZ011989-loaded HSANPs in U937 and HL60 were drawn following nonregression fitting of the absorbance values obtained from the MTT assay (Supporting Information Figure S8 and Supporting Information Figure S9). The IC50 values of EPZ011989-loaded HSANPs estimated on U937 (64 ± 0.1 μM) and HL60 (74 ± 0.1 μM) were significantly lesser than the IC_{50} values calculated for only EPZ011989 on U937 (95 ± 0.1 μM) and HL60 (148 ± 0.3 μM) cells, respectively. Thus, based on these nanoformulation responses, 52 μM concentrations of (54.45 μg/mL) EPZ011989 and equivalent doses of 605.4 μg/mL of DLNP and 550 μg/mL of placebo HSANPs were considered for all of the treatments.

3.4. Suppressed Cell Proliferation and G2/M Phase Cell Cycle Arrest. The EPZ011989-loaded HSANPs with nuclear localization and enhanced cytotoxicity for specific EZH2-positive AML cells were the basis for further investigating the effect on the cell proliferation and cell cycle. Further, the FACS-based measurement of BrdU incorporation vs total DNA content provided the information about cell cycle alteration followed by EPZ011989 and EPZ011989-loaded HSANP and placebo HSANP treatments. The synchronized U937 cells showed the distinct cell cycle G1, S, and G2/M phases with most of the populations in either G1 or S phase in the untreated control. The EPZ011989-loaded HSANP cells were found to exist in the G2/M phase (Figure 4D,F). The PI-based DNA content histogram was fitted with the Watson pragmatic program for quantitative estimation of each cell cycle phase. Interestingly, the cell population appearing inactive in the S phase upon BrdU/PI staining in the untreated control group shifted to the G2/M phase in the EPZ011989-loaded HSANP group (Figure 4E,G). Hence, we can conclude that EPZ011989-loaded HSANPs arrested the AML cells at the G2/M phase and also exhibited significantly higher antiproliferative activity.[36]

To visualize the antiproliferative effect of the EPZ011989-loaded HSANPs, the soft agar colony formation assay was performed for cells treated with placebo HSANPs, EPZ011989, and EPZ011989-loaded HSANPs. The result showed that untreated U937 cells were able to produce larger and multiple colonies at 14 days, whereas cells pretreated with EPZ011989-loaded HSANPs fail to form colonies on soft agar, visualized by the well-known crystal violet staining protocol.[37] The placebo

DOI: 10.1021/acs.molpharmaceut.9b01071
Mol. Pharmaceutics XXXX, XXX, XXX−XXX

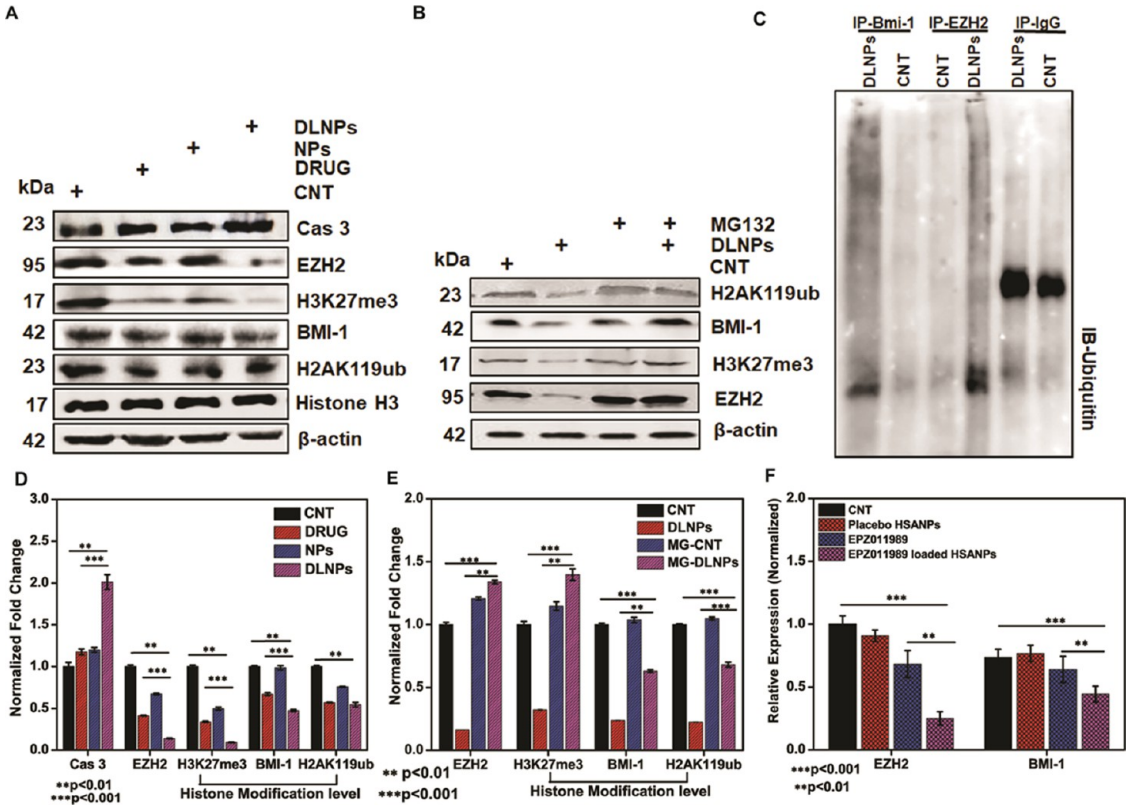

Figure 7. Western blot analysis of control, EPZ011989 (drug), placebo HSANPs (NPs), EPZ011989-loaded HSANPs (DLNPs) for β-actin, caspase 3, EZH2, H3K27me3, BMI-1, and H2AK119Ub (A) and their quantification (D). Western blot analysis after cotreatment of MG132 with EPZ011989 (drug), placebo HSANPs (NPs), and EPZ011989-loaded HSANPs (DLNPs) for β-actin, EZH2, H3K27me3, BMI-1, and H2AK119Ub (B) and their quantification (E); U937 cells were treated as above, 2% total extracts were immunoprecipitated with anti-IgG, anti-EZH2, and anti-BMI-1, and 2% whole extract was taken as input and immunoblotted to detect ubiquitin (D). The β-actin level was used to normalize loading; qPCR analysis of EZH2 and BMI-1 after treatment with control, EPZ011989 (drug), placebo HSANPs (NPs), and EPZ011989-loaded HSANPs (DLNPs) (F). The results were analyzed via one-way ANOVA with the Tukey test at the $^{**}P < 0.01$ and $^{***}P < 0.001$ ($n = 3$) significance levels for statistical comparison.

HSANP- and EPZ011989-exposed cells appeared with comparatively lesser and intermediate-sized colonies on soft agar (Figure 5A,B). The colony formation efficiency (CFE) based on the number of colonies per well was ~8% for the control group, which had been decreased to <1% for the EPZ011989-loaded HSANP-treated group (Figure 5C). The colony formation efficiency was calculated by following already published reports.[38,39] These results showed that EPZ011989-loaded HSANPs exhibit strong antiproliferative activity on AML cells compared to the vehicle and drug mechanistically due to G2/M phase cell cycle arrest, which leads to lesser reproductive potential and results in lesser colonies.

3.5. EPZ011989-Loaded HSANPs Triggered Mitochondrial Damage and Apoptotic Pathway Activation. To analyze the mechanism of AML cell death, the Annexin V-based flow cytometric estimation of apoptosis was performed. The healthy cells stained 6-carboxyfluorescein (6-CFDA)-positive and Annexin V-negative shifted toward an Annexin V-Cy3-positive quadrant after treatment with EPZ011989-loaded HSANPs (33.3%), which was almost double of EPZ011989 (17.3%). However, the placebo HSANPs exerted negligible apoptosis in the U937 population (Figure 6A,C). Next, further analyses showed that the ROS-mediated apoptotic pathway activation triggers with initial mitochondrial membrane depolarization. The FACS-based analysis of the mitochondrial membrane potential was performed by measuring the differential population exhibiting healthy mitochondria with red fluorescence (J-aggregates of JC-1) and with depolarized mitochondrial population exhibiting lower red fluorescence (monomer of JC-1). The shift in the population from red to green in the EPZ011989-loaded HSANP group indicated the associated mitochondrial depolarization, which was significantly higher compared to that in the untreated control and placebo HSANP- and EPZ011989-treated cell populations (Figure 6B,D). Thus, these results confirmed the mechanism of the apoptosis pathways activation, which is firmly associated with mitochondrial damage in leukemic cells.

3.6. Analysis of EZH2 Expression and Downregulation Mechanism. The EPZ011989-loaded HSANPs are specific inhibitors of EZH2; thus, next, we performed the western blot analysis, which demonstrated DLNPs (EPZ011989-loaded HSANPs) mediating suppression of EZH2, BMI-1, H3K27me3, and H2AK119ub and overexpression of caspase 3 (Figure 7A,D). The cotreatment of MG132 (proteasomal pathway inhibitor) with EPZ011989-loaded HSANPs, EPZ011989, placebo HSANPs, and control showed regular expression of EZH2, BMI-1, H3K27me3, and H2AK119ub, indicating the crucial role of proteasomal degradation of EZH2 (Figure 7B,E). The immunoprecipitated EZH2 and BMI-1 following western blot examination with anti-ubiquitin (Ub) indicated the associated polyubiquitination of cellular EZH2 and BMI-1 (Figure 7C). The continuous trailing in the DLNP (EPZ011989-loaded HSANPs) group represents the degree of ubiquitination and temporal degradation. The analysis of results

DOI: 10.1021/acs.molpharmaceut.9b01071
Mol. Pharmaceutics XXXX, XXX, XXX−XXX

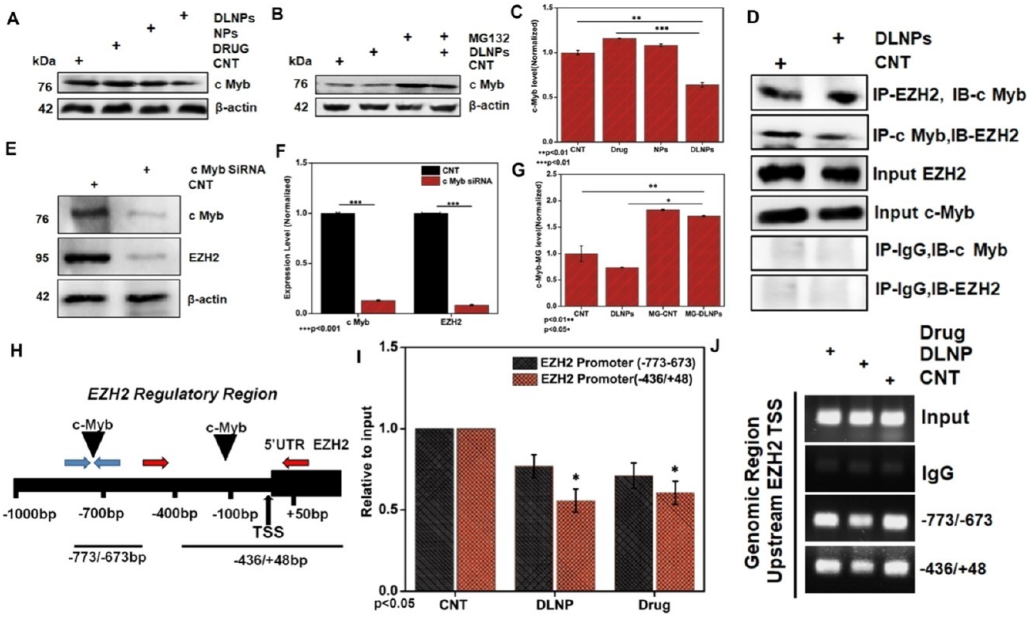

Figure 8. Western blot analysis of control, EPZ011989 (drug), placebo HSANPs (NPs), and EPZ011989-loaded HSANPs (DLNPs) for β-actin and c-Myb (A) and their quantification (C). Western blot analysis after cotreatment of MG132 with EPZ011989 (drug), placebo HSANPs (NPs), and EPZ011989-loaded HSANPs (DLNPs) for β-actin and c-Myb (B) and their quantification (G). Immunoprecipitation study to analyze the interaction between c-Myb and EZH2 in 2% total extracts after control, EPZ011989 (drug), placebo HSANP (NPs), and EPZ011989-loaded HSANP (DLNPs) treatment (D). c-Myb siRNA silencing mechanism after treatment with c-Myb siRNA and western blot analysis for c-Myb and EZH2 (E, F). The results were analyzed via one-way ANOVA with the Tukey test at the $^{*}P < 0.05$, $^{**}P < 0.01$, and $^{***}P < 0.001$ ($n = 3$) significance levels. The two EZH2 promoter region −773/−673 and −436/+48 sequences represent the c-Myb interaction site on the EZH2 promoter (H). The qPCR analysis after ChIP is quantitatively represented (I). The visualization of qPCR end products on 2% agarose gel (J).

shows enhanced polyubiquitination of EZH2 in EPZ011989-loaded HSANPs in comparison to the untreated control, and anti-IgG IP showed no association of ubiquitin in WB, suggesting assay specificity (Figure 7C). The gene expression pattern in the leukemic cell line was analyzed by real-time PCR representing significant downregulation of EZH2 and BMI-1 genes following EPZ011989-loaded HSANP treatment compared to EPZ011989 and untreated control (Figure 7F).

3.7. Analysis of Attenuating EZH2 and c-Myb Interaction. We examined the c-Myb and EZH2 protein level in the AML cells upon EPZ011989-loaded HSANPs exposure to check whether it interferes with protein expression level of transcription factor c-Myb and EzH2 expression. Interestingly, EPZ011989-loaded HSANPs inhibited c-Myb protein expression in the U937 cell line (Figure 8A,C). Indeed, a reversal of c-Myb protein loss by the proteasomal inhibitor (MG132) indicates that EPZ011989-loaded HSANPs target c-Myb by promoting the proteasomal degradation (Figure 8B,G) because reduced c-Myb expression is correlated with lower EZH2 levels (Figure 7A). The physical interaction between c-Myb and EZH2 is identified by immunoprecipitation, and the result confirmed the functional interaction between EZH2 and c-Myb at the cellular level (Figure 8C). Next, the 2% total extract immunoprecipitated after treatment with EPZ011989-loaded HSANPs and confirmed the physical interaction between EZH2 and c-Myb at the protein level.

3.8. c-Myb as a Direct Modulator of the EZH2 Expression. Next, we have investigated the modulatory role of transcription factor c-Myb in controlling EZH2 expression in AML cells. Thus, siRNA-mediated RNAi was used to knockdown the cellular level of c-Myb with subsequent measurement of EZH2 expression using western blotting. The results showed the significant downregulation of cellular EZH2 upon c-Myb silencing (Figure 8E,F). Further, we investigated whether the expression of EZH2 was directly modulated by c-Myb. A search of the human EZH2 promoter sequence in transcription factor binding site databases (i.e., database TRANCFAC_8.3) indicated the presence of putative c-Myb binding sites, suggesting that EZH2 might be a direct target of c-Myb. However, for the definitive validation of direct interaction of the EZH2 promoter with c-Myb protein, the chromatin immunoprecipitation (ChIP) assay was performed on the U937 cell isolates. The qPCR of the recovered templates from the ChIP assay using specific EZH2 promoter-specific primers confirmed the c-Myb occupancy on the EZH2 promoter (Figure 8H). For the full length of the EZH2 promoter (−1702 to +52), we have used two different primer sets specific to the EZH2 promoter from −773/−673 and −436/+48 with amplicon sizes of 100 and 484 bp, respectively (Supporting Information Figure S10). These two different primers were prevalidated for the amplification of the specific EZH2 region in previously published method.[40,41] The EZH2 gene showed enrichment of c-Myb compared to the IgG control. The specific binding of c-Myb on the EZH2 promoter region −773/−673 and −436/+48 sequences is displayed in the amplification plot obtained on qPCR (Figure 8I), which were further confirmed by visualization on 2% agarose gel (Figure 8J). The c-Myb protein can modulate the EZH2 expression; hence, the levels of the associated transcripts were screened following DLNP, EPZ011989, and untreated control group isolates of U937 cells (Supporting Information Figure S11). The overall result concludes that the knockdown of c-Myb expression causes significant downregulation of EZH2 and indicates that c-Myb can modulate the EZH2 expression by binding on its promoter sequence.

DOI: 10.1021/acs.molpharmaceut.9b01071
Mol. Pharmaceutics XXXX, XXX, XXX−XXX

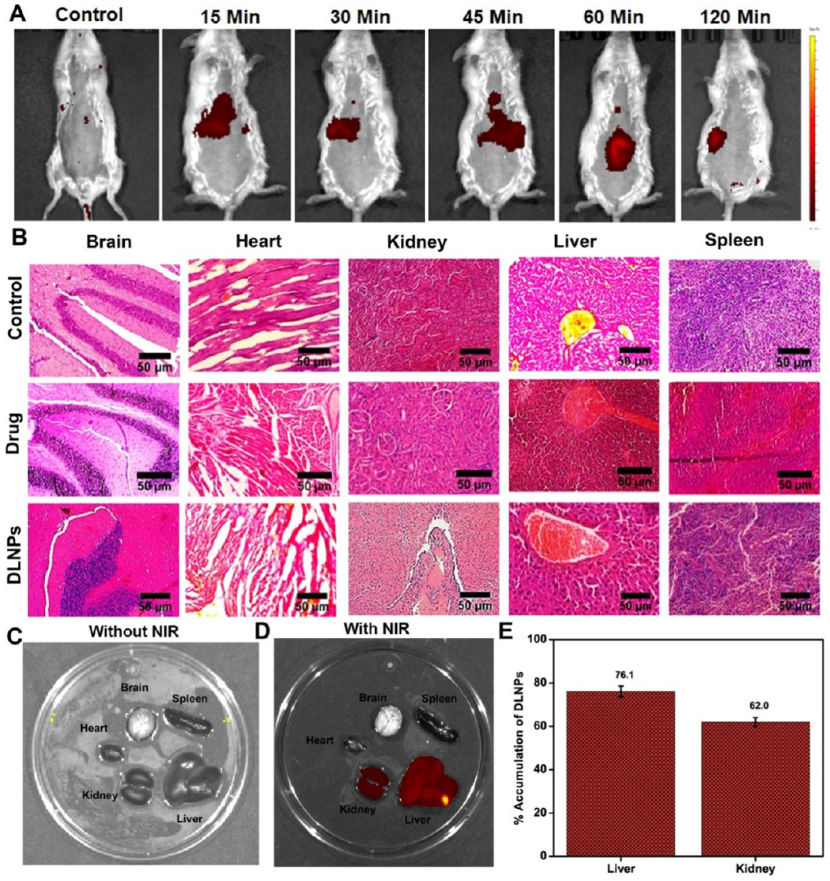

Figure 9. In vivo biodistribution of fluorescent-tagged nanoformulation, images acquired at 15, 30, 45, 60, and 120 min post intravenous injection (A). The histopathological analysis of heart, kidney, liver, spleen, and brain sections following H&E staining (scale bar = 50 μm) (B). Ex vivo imaging of organs harvested at 2 h post-injection (C, D) and quantitation of % accumulation of DLNPs in significant organs (E).

3.9. In Vivo and ex Vivo Biodistribution of Nanoformulation. To study in vivo biodistribution, ICG-tagged EPZ011989-loaded HSANPs were intravenously injected in BALB/c mice. The time-dependent images were acquired on an animal imager (IVIS, spectrum) in the near-infrared (NIR) region (Figure 9A). The strong NIR fluorescence emission and penetration ability in the deep tissues without causing any significant heating are the characteristics for the potential use of ICG as an in vivo dye.[42] The mice exposed to the formulation showed the gradual retention in the liver, which was maximum in 45 min post-injection. The fast excretion of the nanomaterial from the animal system was solely dependent on the nanoparticle size and physicochemical characteristics. Further, at the end of 2 h, the signals from the kidney indicated the systemic clearance with continuous clearance from the hepatic systems. The ex vivo imaging of the kidney, spleen, liver, brain, and heart (Figure 9C) has shown the significant accumulation of EPZ011989-loaded HSANPs in the liver and kidney (Figure 9D). However, the heart, kidney, liver, spleen, and brain isolated from the mice with prolonging treatment of the EPZ011989 and EPZ011989-loaded HSANPs have shown negligible morphological damage assessed after hematoxylin and eosin staining (Figure 9B). Thus, these results confirmed the systemic compatibility of the EPZ011989-loaded HSANPs showing optimal retention, fast excretion, and negligible nonspecific toxicity to the organs.

3.10. In Vivo Therapeutic Assessment on AML Xenograft Model. The engraftment of the U937 leukemic cells in the nude mice model was established by injecting these cells via the tail vein, which demonstrated the antileukemic effect of EPZ011989-loaded HSANPs. The mice (n = 15) were injected with the U937 AML cell line for induction of the xenograft model of AML (Figure 10A). After the 20th day of injection of leukemic cells, all mice peripheral blood was assessed for the successful development of the AML model. Following treatment of EPZ011989, placebo HSANPs, and EPZ011989-loaded HSANPs, the body weight of the animal was recorded, and all of the mice were euthanized on the 29th day and characterized using FACS-based immunophenotyping for specific $CD45^+$ and $CD11b^+$ markers from peripheral blood and bone marrow samples. The continuous dosing of the EPZ011989-loaded HSANPs leads to a significant decrease in the leukemic cell population compared to control and the EPZ011989-injected group (Figure 10B). The whole population of human $CD45^+$ (common leukocyte antigen) leucocyte and $CD11b^+$ was significantly increased in the AML model (Figure 10B,G), suggesting that EPZ011989-loaded HSANPs conferred strong regulatory effect on the leukemic cell transformation in nude mice. Subsequently, the measure of the splenomegaly as a function of size, which is associated with hematological malignancy, was examined for EPZ011989-loaded HSANPs, EPZ011989, and placebo HSANPs-treated AML-bearing nude mice. The significant enlargement of the spleen in the AML model was observed, which was not seen in the EPZ011989-loaded HSANPs, whereas intermediate enlargement of the spleen was there in the EPZ011989 and control

DOI: 10.1021/acs.molpharmaceut.9b01071
Mol. Pharmaceutics XXXX, XXX, XXX−XXX

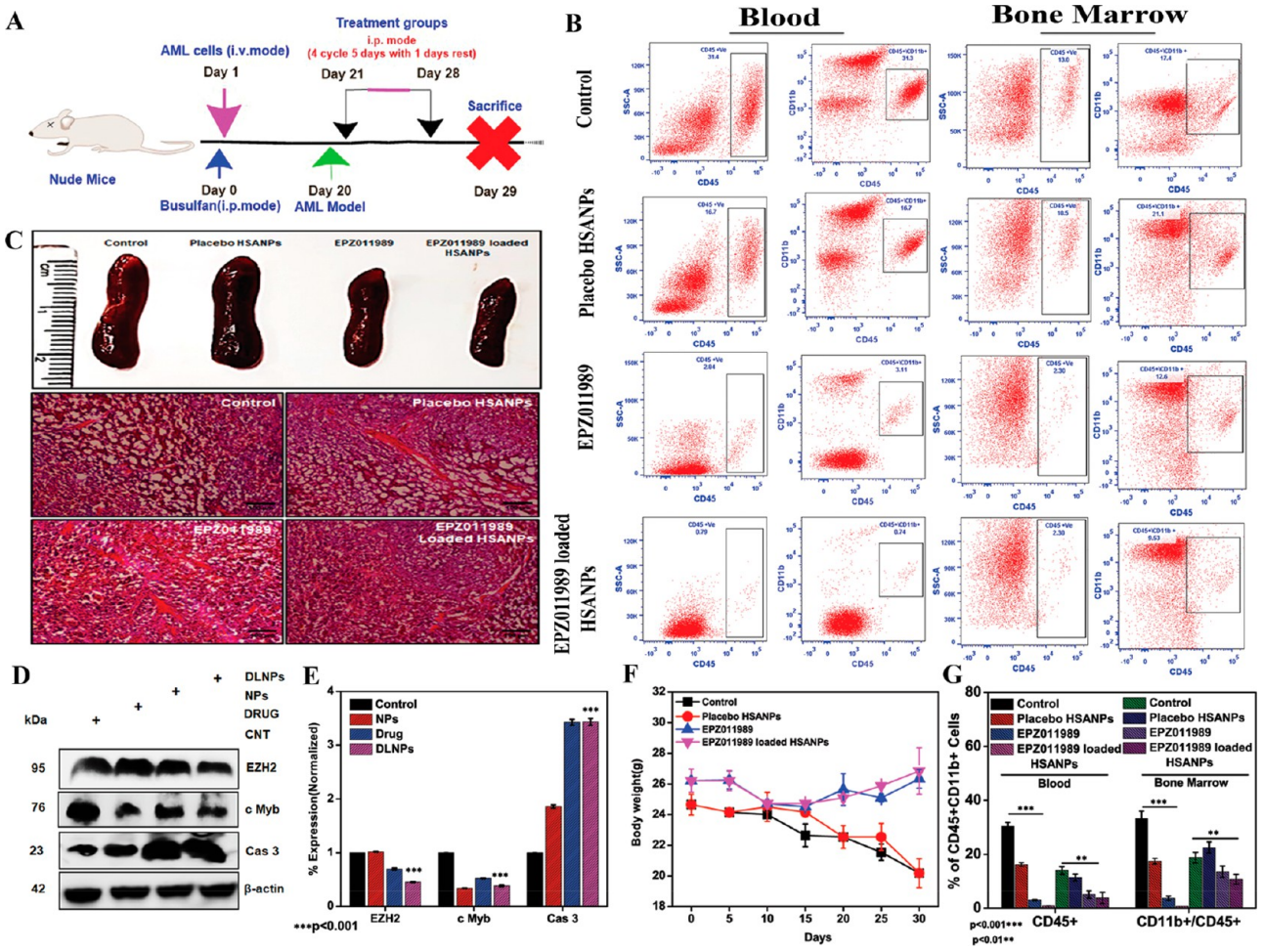

Figure 10. Therapeutic efficacy of EPZ011989-loaded HSANPs on the xenograft model of acute myeloid leukemia. The schematic diagram of the AML xenograft model preparation and therapeutic assessment (A). The dual $CD11b^+$ and $CD45^+$ positive cell populations were estimated using FACS in peripheral blood and bone marrow samples obtained from nanoformulation-injected mice (B). The quantitative representation of the $CD11b^+$ and $CD45^+$ positive cell populations isolated from differently injected mice (G). The physical description of the set of spleens isolated from mice administered with different groups (C). The downregulation of EZH2 and c-Myb and overexpression of caspase 3 examined using western blotting considering β-actin as control (D). The change in the body weight following placebo HSANPs, EPZ011989, and EPZ011989-loaded HSANPs administration considering un-injected control represented in scattered plot (F). The data represent the mean ± standard deviation ($n = 3$) and compared using one-way ANOVA with the Tukey test at the $^{**}P < 0.01$ and $^{***}P < 0.001$ significance levels for statistical comparison.

nude mice (Figure 10C). To confirm the action of the encapsulated drug, the protein levels of EZH2, c-Myb, and caspase 3 in the leukemic cell isolates were analyzed using western blotting. The results confirmed the consistent inhibitory action of EPZ011989-loaded HSANPs in the AML model, with significant downregulation of EZH2 and c-Myb and overexpression of caspase 3 (Figure 10D,E). The overall results demonstrated better efficacy of EPZ011989-loaded HSANPs in targeting the AML with significant downregulation of the EZH2 and c-Myb expression, turning a new epigenetic target for AML therapy.

4. DISCUSSION

The current study showed that the HSA nanoformulation had overcome major limitations associated with free EPZ011989, such as poor solubility and low bioavailability with better efficacy for AML treatment. For the preparation of EPZ011989-loaded HSANPs, the optimization with HSA concentration, magnetic stirring, and temperature was done to obtain narrower particle size distribution by the desolvation method. The nanodimensional size with spherical morphology made HSANPs as EPZ011989-loaded HSANPs a suitable drug carrier. The calculated loading efficiency and entrapment efficiency of EPZ011989 into HSA nanoformulation characterized it as a suitable carrier system for AML treatment. The functional group analysis revealed the crucial interactions and chemical modifications during the preparation process of EPZ011989-loaded HSANPs. The crucial interaction at the amide I peak in FTIR indicated EPZ011989 interaction with HSA during encapsulation. Moreover, the physical state and stoichiometric analysis suggest EPZ011989 encapsulation into HSANPs. The characteristics of HSANPs such as smaller size, higher monodispersed phase, reproducibility, and ease to scale up in the preparation involving less time, and lower expenses make it suitable as a drug delivery vehicle.

The biophysical and in silico studies revealed the predominating noncovalent interactions between HSANPs and EPZ011989. Interestingly, the UV spectral absorbance and steady-state tryptophan fluorescence emission intensity primarily indicated the absence of any physical covalent interactions between HSA and EPZ011989. The in silico and biophysical investigations revealed major noncovalent interactions between

DOI: 10.1021/acs.molpharmaceut.9b01071
Mol. Pharmaceutics XXXX, XXX, XXX−XXX

HSA and EPZ011989 as the basis of carrier and drug compatibility.

Circular dichroism spectroscopy results further revealed the conformational change in the protein secondary structure during nanoparticle synthesis, from α-helix to the β-sheet and random coils, indicating a degree of structural change giving specific morphology, stability, and functionality to HSANPs. The improved in vitro drug release profile showed the characteristics of preferred drug carriers. The nanoformulation minimizes off-target release and nonspecific side effects during circulation and also prevents efflux from resistant cells. The cumulative drug release pattern from the nanoformulation may be similar to the EPZ011989 release after internalization in AML cells, downregulating the expression of EZH2 and associated genes, triggering cumulative epigenetic alterations.

The increased solubility profile EPZ011989-loaded HSANPs significantly indicates that EPZ011989-loaded HSANPs are able to overcome the aqueous solubility problem of free EPZ011989. The stability study shows the compatibility and stability of the EPZ011989-loaded HSANPs in various physiological fluid conditions. The rhodamine-tagged EPZ011989-loaded HSANPs show that the localization into the nucleus might be due to the conjugation of EPZ011989 (drug) into the HSANP nanoformulation targeting its delivery toward the nucleus and binding to the DNA-binding histone proteins. This can be compared with the evidence where histone deacetylase (HDAC) inhibitors serve as a tag for translocating the nanostructures into the nucleus and triggering a superior effect. For instance, prostate cancer was targeted utilizing histone deacetylase inhibitor (HDACi), which inhibited isoforms of HDAC by varying the nuclear localization controlling HDAC activity.[43] Other inhibitors' target resides in the nucleus with binding to DNA or histone protein and allowing the translocation of the nanoparticle from the cytosol to the nucleus. Self-localization of the particle in the nucleus of the cells activates the gene expression mediated by the induction of histone acetyltransferase (HAT) activity.[44] EZH2 is responsible for chromatin compaction by transferring methyl groups to lysine residues of the histone protein, the reversibility by EPZ011989 in inhibiting this histone methyl lysine transferase EZH2, and thereby reducing the availability of the methyl group for histone methylation. All phenomena are localized in the nucleus, so the action of EPZ011989 directed toward histone is predicted.

Accumulation of HSANPs in leukemic cells could be attributed to leaky tumor capillary and defective lymphatic drainage. Transcytosis of HSANPs through endothelial receptor gp60 (60 kDa glycoprotein) and bonding facilitates caveolae and SPARC (43 kDa glycoprotein overexpressed in cancer cells)-mediated intracellular uptake.[45] Finally, HSANPs protect EPZ011989 from biodegradation, allow escape from lysosomal entrapment, and expedite controlled release, allowing nuclear entry and thereby downregulation of EZH2 gene expression, resulting in rehabilitation of characteristic epigenetic alterations. Subcellular localization of HSANPs is also evident in the clathrin-mediated cellular uptake in cancer (in vitro and in vivo).[46] The superior cytotoxicity of DLNPs (EPZ011989-loaded HSANPs) could be due to the EPZ011989-based targeting of the AML cells to the nucleus and local release of EPZ011989 from the nanoformulation. This minimal dose is sufficient to induce the cytotoxic effect in the U937 and HL60 cell lines without any significant impact on the noncancer cells and could be a promising therapeutic strategy in reverting epigenetic modifications for AML prevention. The nuclear localization might affect the AML nuclear function, which was confirmed by measuring the active -S cell cycle phase using immunostaining of the incorporated BrdU (5′bromo-2′deoxy-uridine) corroborated with propidium iodide-based DNA content analysis.[47] The in vitro synchronization was done to arrest cultured cells in specific phases of the cell cycle stage before using them for screening the agent affecting the regular cell cycle progression. The presence of all of the test cells in the single cell cycle stage provides a better assessment with minimum noise/error contribution in the estimated results.[31] The presence of the active S phase is associated with the higher proliferation of AML cell populations with higher incorporation of the BrdU signified presence or absence of DNA synthesis.[48] The EPZ011989-loaded HSANPs promoting the G2/M phase cell cycle arrest with a negligible active S phase population is the basis of the antiproliferative potential. The cell cycle is one of the measures of epigenetic inhibition besides the antitumor activity of the chemotherapeutic drug; it minimizes the accumulation of mutations and abnormal growth. The crosstalk of PRC2 and cyclin-dependent kinases for the regulation of the cell cycle is evident in hematologic malignancies, which further suggests targeting EZH2 as a potential strategy for inducing tumor suppression and inhibition of AML explicitly.[49] The colony formation assay measures the ability of the cells in culture to grow and divide into groups and also provide an indirect measurement of cell death. For the suspension cells that move freely in the media, the colony forming ability determines the ability to restrict the large-scale movement of the cells in solid matrices (soft agar).[50] Here, our results confirmed that EPZ011989-loaded HSANP-treated U937 cells are not able to generate and form colonies with underlying mechanism supported by the effect of DZNep (EZH2 inhibitor) on in vitro colony formation assays on soft agar, demonstrated to test the sensitivity of AML cells with EZH2 loss-of-function mutations.[51] The exposure of cells to EPZ011989-loaded HSANPs was associated with significant repression of cell growth by a decline in the number of colonies as compared to the control and drug and was supported well by the reported results of the HSA−vorinostat complex, which inhibits the colony proliferation capability of leukemic cells.[33,52]

To analyze the actual mechanism of AML cytotoxicity, we evaluated the apoptosis induction by EPZ011989-loaded HSANPs in AML cells in comparison to EPZ011989 and placebo HSANPs. The EPZ011989-loaded HSANPs induce apoptosis in most of the population. Both the JC-1- and MTT-based assays are linked to the mitochondrial function and provide two different response mechanisms based on the target and measurement methodologies.[53] The MTT assay measures the metabolic activity as function of hyper metabolic and lower metabolic cellular state that can be linked to the mitochondrial enzyme activity. However, JC-1 measures the mitochondrial membrane potential under stress, and it gets depolarized, which can be linked with the opening of the mitochondrial transition pore, generation of ROS, release of cytochrome c, and initiation of the caspase 3-independent pathway of apoptosis.[54] The overall results suggested the activation of both caspase-dependent and caspase-independent activation of the apoptosis pathways exerting anti-AML activity.

As already reported, EPZ011989 treatment was more sensitive to EZH2 inhibition in BAP1-mutant cell lines, both in two-dimensional (2D) and 3D cultures.[55] The use of drugs targeting epigenetic modifiers or pharmacologic inhibition of

DOI: 10.1021/acs.molpharmaceut.9b01071
Mol. Pharmaceutics XXXX, XXX, XXX−XXX

EZH2 is a highly promising strategy in selected target diseases[56] and may have potential benefits in the treatment of AML. The downregulation of EZH2 expression in the leukemic cells (U937) was evident in synovial sarcoma (Fuji and HS-SY-II), and soft tissue sarcoma (SW982) cell lines against EPZ011989 treatment are already reported.[57] Notably, for the first time, the EPZ011989-loaded HSANP treatment in acute myeloid leukemia demonstrated enhanced regulation with superior sensitivity against EZH2. DLNP (EPZ011989-loaded HSANPs)-mediated downregulation of EZH2, BMI-1, H3K27me3, and H2AK119Ub and overexpression of caspase 3 indicated a mutual link between PcG complex activity and apoptotic pathways. Mechanistically, EZH2 serves as a methyltransferase and results in trimethylation of H3 at the K27 position. Reported results showed that EZH2 knockdown results in a significant decrease in cellular proliferation, suggesting that epigenetic therapy targeting PcG machinery and the development of drugs inhibiting trimethylation of lysine 27 on H3K27me3 can be an effective therapy.[58] The downregulation of PRC1 complex member BMI-1 post-DLNP treatment suggested a mutual functional role of both complexes in the silencing process. The PRC1 complex monoubiquitinates H2A at the K119 position and directs it for silencing and is evident that BMI-1 as the PRC1 component overexpressed in acute myeloid leukemia patients contributes to leukemogenesis.[16] The EPZ011989-loaded HSANPs exerted reduction of PcG by regulating EZH2 directly and BMI-1 via indirect mechanisms. Thus, our findings are consistent with observations in other cell types and demonstrated that HSANPs as a drug carrier triggers a superior control over PcG by mutually downregulating both the PRC1 and PRC2 complexes.[59−61]

The protein ubiquitination is directed toward proteasomal degradation and maintains the functional homeostasis of the cells.[62] The increased polyubiquitination of EZH2 and BMI-1 after DLNP exposure indicates superior targeting of the PcG complexes by elicited proteasomal degradation. Remarkably, the indirect downregulation of BMI-1 could be because of the fact that EZH2-mediated reduced level of H3K27me3 at the chromatin binding site avails minimum docking site for PRC1 subunit BMI-1 binding, thus triggering downregulation of the alternative PRC complex. Further, the role of proteasomal degradation machinery was confirmed by restored expression of EZH2, BMI-1, H3K27me3, and H2AK119ub after MG132 and DLNP cotreatment, indicating a crucial role of polyubiquitination and proteasomal degradation. In our results, increased polyubiquitination of EZH2 and BMI-1 after EPZ011989-loaded HSANP treatment indicates the novel targeting of the PcG complexes by elicited proteasome degradation for AML retardation.

The central role of transcription factor c-Myb has been shown in the development and progression of AML, and c-Myb is highly expressed in immature hematopoietic progenitor cells and is required for definitive hematopoiesis and maintenance of adult hematopoietic stem cell self-renewal.[63] Most acute myeloid and lymphoid leukemic cells overexpress c-Myb.[64] Notably, c-Myb is another indirect target of EPZ011989-loaded HSANPs, which is being investigated for the first time in the context of nanoformulation-based targeting. Indeed, a reversal of DLNP-responsive downregulation of the c-Myb protein was restored after MG132 treatment, thus correlating the reduced c-Myb expression with lower EZH2 levels. These results have raised the possibility that inhibition of c-Myb might be able to eradicate the leukemic cells and also provide a new c-Myb-based therapeutic approach for the treatment of AML.

Furthermore, siRNA-mediated silencing of c-Myb expression significantly downregulating the EZH2 expression and indicating the crucial functional interaction is for the first time reported in this study, whereas the association of c-Myb with BMI-1 was demonstrated in Z-181 and SUP-B15 cells.[65] Moreover, crucial interaction between EZH2 and c-Myb at the protein level suggests that EZH2 might be a direct c-Myb target. These results indicate that expressions of c-Myb and EZH2 are functionally related and the c-Myb-EZH2 pathway could play a role in regulating the proliferation and survival of acute myeloid cells. The regulation of the EZH2 gene and the central role of c-Myb in hematopoiesis are further confirmed by chromatin immunoprecipitation, concluding that c-Myb directly binds at the EZH2 promoter site and thus regulating its expression. Our results also represent the mechanistic similarity with the already reported studies of the ETS transcription factor binding to the EZH2 promoter in prostate cancer.[41] In another study, STAT3, a transcriptional factor, induced EZH2 activation by binding to the specific Stat3 motif of the EZH2 promoter region.[40] Altogether, these results suggest that expressions of c-Myb and EZH2 are functionally related and the c-Myb-EZH2 pathway plays a significant role in regulating the proliferation and survival of AML cells. The promising antileukemic activity of EPZ011989-loaded HSANPs revealed by the present study also supports the fact that it is a potent inhibitor of c-Myb-EZH2 interaction and makes a new platform for the treatment of AML by regulation of proliferation and survival of AML cells through epigenetic machinery-mediated ubiquitination and proteasomal degradation.

Considering the above-mentioned molecular mechanism, the in vivo whole-body distribution in the BALB/c mice showed initial systemic circulation and availability of DLNPs, followed by major accumulation in the kidney and liver in later hours. This reconfirms systemic and visceral clearance, and quantification data have shown that they mostly accumulate in the kidney and liver. The representative microscopic observations have shown negligible toxicities in the heart, kidney, liver, spleen, and brain tissue in comparison to the control group, implying the low toxicity and excellent biocompatibility of EPZ011989 and EPZ011989-loaded HSANPs in vivo. Overall, these findings suggest that EPZ011989-loaded HSANPs act as a potentially promising therapeutic target for controlling polycomb expression in AML treatment and show excellent aqueous dispersibility and biocompatibility with the in vivo system. The in vivo therapeutic efficacy of EPZ011989-loaded HSANPs was assessed in the xenograft model of AML in nude mice. Based on the available data, this is the first study to demonstrate the in vivo therapeutic relevance of EPZ011989-loaded HSANPs in a nude xenograft model of AML. The FACS-based immunophenotyping of $CD45^+$ myeloid cell and $CD11b^+$ monocyte cell populations remains the primary modality to diagnose AML. On treating with EPZ011989-loaded HSANPs, the expression of both markers decreased in blood and bone marrow samples, showing the better efficacy of the nanoformulation in inhibiting the proliferation and transformation by targeting EZH2. The absence of spleen enlargement in EPZ011989-loaded HSANPs in the AML model indicated the controlled leukemic population in the animal,[66] and the histopathological assessment of the hematoxylin and eosin (HE)-stained spleen sections showed negligible morphological damage in nanoformulation-treated animals. Moreover, the downregulation of EZH2 and c-Myb and

DOI: 10.1021/acs.molpharmaceut.9b01071
Mol. Pharmaceutics XXXX, XXX, XXX−XXX

overexpression of caspase 3 in isolated leukemic population confirmed the in vivo efficacy of EPZ011989-loaded HSANPs in the treatment of AML. Overall assessment of the therapeutic efficacy on the in vivo AML model demonstrated newer approaches of nanoformulation-based epigenetic targeting of AML and great translational potential for AML therapy.

5. CONCLUSIONS

In summary, the prepared EPZ011989-loaded HSANPs eliminate the solubility and stability problems associated with free drug and trigger superior antileukemic activity via the antiproliferative effect. Mechanistically, the downregulation of EZH2 and indirect targeting of BMI-1 and c-Myb are established as the basis of the collective epigenetically targeted anti-AML activity. The ubiquitination and proteasomal degradation attenuate the crucial interactions and cellular levels of EZH2 and c-Myb proteins. The siRNA-based silencing of c-Myb confers a lower expression of EZH2, confirmed for cellular interaction at the protein level, which is further established as a direct regulator that binds explicitly to the EZH2 promoter. In addition to the mechanism of action, the present nanoformulation has shown higher systemic compatibility with negligible nonspecific toxicity. The reduced population of leukemic cells ($CD45^+$ and $CD11b^+$) upon nanoformulation exposure, confirmed for lower EZH2 and c-Myb protein levels, demonstrated a novel therapeutic approach for epigenetic targeted anti-AML therapy.

■ ASSOCIATED CONTENT

Supporting Information

The Supporting Information is available free of charge at https://pubs.acs.org/doi/10.1021/acs.molpharmaceut.9b01071.

In silico docking result; primers used for real-time PCR and CHIP assay; atomic force microscopy (AFM) images; FTIR spectra, XRD pattern, CD spectroscopy, differential scanning calorimetric (DSC) curves, UV visible spectroscopy, fluorescence spectroscopy results of HSA, placebo HSANPs, EPZ011989, and EPZ011989-loaded HSANPs; EPZ011989 standard curve; nanoformulation stability analysis; cellular uptakes in U937 cells; dose−response curve of formulations on U937 cells and Hl60 cells; and ChIP assay by qPCR (PDF)

■ AUTHOR INFORMATION

Corresponding Author

*E-mail: subhasreerc@inst.ac.in. Phone: +91-172-2210075/57/56. Fax: +91-172-2211074.

ORCID

Surajit Karmakar: 0000-0001-6800-2457

Subhasree Roy Choudhury: 0000-0001-7894-8297

Notes

The authors declare no competing financial interest.

■ ACKNOWLEDGMENTS

We would like to thank the Science and Engineering Research Board (SERB) grant YSS/2015/001706 for financial support.

■ ABBREVIATIONS

AML, acute myeloid leukemia; PcG, polycomb group; EZH2, enhancer of zeste homologue 2; HSA, human serum albumin; DLS, dynamic light scattering; TEM, transmission electron microscopy; EZH2, enhancer of zeste homologue 2; FESEM, field emission electron microscopy; AFM, atomic force microscopy; CD, circular dichroism; DSC, differential scanning calorimetry; HSANPs, human serum albumin nanoparticles; VDW, Van der Waals forces

■ REFERENCES

(1) Papakonstantinou, N.; Ntoufa, S.; Chartomatsidou, E.; Kotta, K.; Agathangelidis, A.; Giassafaki, L.; Karamanli, T.; Bele, P.; Moysiadis, T.; Baliakas, P.; Sutton, L. A.; Stavroyianni, N.; Anagnostopoulos, A.; Makris, A. M.; Ghia, P.; Rosenquist, R.; Stamatopoulos, K. The histone methyltransferase EZH2 as a novel prosurvival factor in clinically aggressive chronic lymphocytic leukemia. *Oncotarget* **2016**, *7*, 35946−35959.

(2) Gerstung, M.; Papaemmanuil, E.; Martincorena, I.; Bullinger, L.; Gaidzik, V. I.; Paschka, P.; Heuser, M.; Thol, F.; Bolli, N.; Ganly, P.; Ganser, A.; McDermott, U.; Dohner, K.; Schlenk, R. F.; Dohner, H.; Campbell, P. J. Precision oncology for acute myeloid leukemia using a knowledge bank approach. *Nat. Genet.* **2017**, *49*, 332−340.

(3) Villanueva, M. T. Genetics: Acute myeloid leukaemia: driving the driver. *Nat. Rev. Cancer* **2016**, *16*, No. 479.

(4) Coombs, C. C.; Tallman, M. S.; Levine, R. L. Molecular therapy for acute myeloid leukaemia. *Nat. Rev. Clin. Oncol.* **2016**, *13*, 305−318.

(5) Grove, C. S.; Vassiliou, G. S. Acute myeloid leukaemia: a paradigm for the clonal evolution of cancer? *Dis. Model Mech.* **2014**, *7*, 941−951.

(6) Venton, G.; Labiad, Y.; Colle, J.; Fino, A.; Afridi, S.; Torres, M.; Monteuil, S.; Loriod, B.; Fernandez-Nunez, N.; Farnault, L.; Suchon, P.; Mattei, J. C.; Rihet, P.; Bergon, A.; Nguyen, C.; Baier, C.; Costello, R. Natural killer cells in acute myeloid leukemia patients: from phenotype to transcriptomic analysis. *Immunol. Res.* **2016**, *64*, 1225−1236.

(7) Siegel, R.; Naishadham, D.; Jemal, A. Cancer statistics, 2012. *Ca-Cancer J. Clin.* **2012**, *62*, 10−29.

(8) Estey, E. H. CME Information: Acute myeloid leukemia: 2014 update on risk-stratification and management. *Am. J. Hematol.* **2014**, *89*, 1063−1081.

(9) Lin, T. L.; Levy, M. Y. Acute myeloid leukemia: focus on novel therapeutic strategies. *Clin. Med. Insights: Oncol.* **2012**, *6*, 205−217.

(10) Fathi, A. T.; Wander, S. A.; Faramand, R.; Emadi, A. Biochemical, Epigenetic, and Metabolic Approaches to Target IDH Mutations in Acute Myeloid Leukemia. *Semin. Hematol.* **2015**, *52*, 165−171.

(11) Geiger, T. L.; Rubnitz, J. E. New approaches for the immunotherapy of acute myeloid leukemia. *Discov. Med.* **2015**, *19*, 275−284.

(12) Abdel-Wahab, O.; Levine, R. L. Mutations in epigenetic modifiers in the pathogenesis and therapy of acute myeloid leukemia. *Blood* **2013**, *121*, 3563−3572.

(13) Levine, S. S.; King, I. F.; Kingston, R. E. Division of labor in polycomb group repression. *Trends Biochem. Sci.* **2004**, *29*, 478−485.

(14) Bird, A. DNA methylation patterns and epigenetic memory. *Genes Dev.* **2002**, *16*, 6−21.

(15) Herviou, L.; Cavalli, G.; Cartron, G.; Klein, B.; Moreaux, J. EZH2 in normal hematopoiesis and hematological malignancies. *Oncotarget* **2016**, *7*, 2284−2296.

(16) Sawa, M.; Yamamoto, K.; Yokozawa, T.; Kiyoi, H.; Hishida, A.; Kajiguchi, T.; Seto, M.; Kohno, A.; Kitamura, K.; Itoh, Y.; Asou, N.; Hamajima, N.; Emi, N.; Naoe, T. BMI-1 is highly expressed in M0-subtype acute myeloid leukemia. *Int. J. Hematol.* **2005**, *82*, 42−47.

(17) Lund, K.; Adams, P. D.; Copland, M. EZH2 in normal and malignant hematopoiesis. *Leukemia* **2014**, *28*, 44−49.

(18) Göllner, S.; Muller-Tidow, C. Inhibition of EZH2 degradation as a novel approach to overcome drug resistance in acute myeloid leukemia. *Mol. Cell. Oncol.* **2017**, *4*, No. e1291396.

(19) Myung, J.; Kim, K. B.; Crews, C. M. The ubiquitin-proteasome pathway and proteasome inhibitors. *Med. Res. Rev.* **2001**, *21*, 245−273.

(20) Gopal, V.; Hulette, B.; Li, Y. Q.; Kuvelkar, R.; Raza, A.; Larson, R.; Goldberg, J.; Tricot, G.; Bennett, J.; Preisler, H. c-myc and c-myb

DOI: 10.1021/acs.molpharmaceut.9b01071
Mol. Pharmaceutics XXXX, XXX, XXX−XXX

expression in acute myelogenous leukemia. *Leuk. Res.* **1992**, *16*, 1003−1011.
(21) Uttarkar, S.; Dasse, E.; Coulibaly, A.; Steinmann, S.; Jakobs, A.; Schomburg, C.; Trentmann, A.; Jose, J.; Schlenke, P.; Berdel, W. E.; Schmidt, T. J.; Muller-Tidow, C.; Frampton, J.; Klempnauer, K. H. Targeting acute myeloid leukemia with a small molecule inhibitor of the Myb/p300 interaction. *Blood* **2016**, *127*, 1173−1182.
(22) Wouters, B. J.; Delwel, R. Epigenetics and approaches to targeted epigenetic therapy in acute myeloid leukemia. *Blood* **2016**, *127*, 42−52.
(23) Campbell, J. E.; Kuntz, K. W.; Knutson, S. K.; Warholic, N. M.; Keilhack, H.; Wigle, T. J.; Raimondi, A.; Klaus, C. R.; Rioux, N.; Yokoi, A.; Kawano, S.; Minoshima, Y.; Choi, H. W.; Porter Scott, M.; Waters, N. J.; Smith, J. J.; Chesworth, R.; Moyer, M. P.; Copeland, R. A. EPZ011989, A Potent, Orally-Available EZH2 Inhibitor with Robust in Vivo Activity. *ACS Med. Chem. Lett.* **2015**, *6*, 491−495.
(24) Wan, X.; Zheng, X. Y.; Pang, X. Y.; Zhang, Z. M.; Jing, T.; Xu, W.; Zhang, Q. Z. The potential use of lapatinib-loaded human serum albumin nanoparticles in the treatment of triple-negative breast cancer. *Int. J. Pharm.* **2015**, *484*, 16−28.
(25) Fanali, G.; di Masi, A.; Trezza, V.; Marino, M.; Fasano, M.; Ascenzi, P. Human serum albumin: From bench to bedside. *Mol. Aspects Med.* **2012**, *33*, 209−290.
(26) Kratz, F. Albumin as a drug carrier: Design of prodrugs, drug conjugates and nanoparticles. *J. Controlled Release* **2008**, *132*, 171−183.
(27) Quan, Q.; Xie, J.; Gao, H. K.; Yang, M.; Zhang, F.; Liu, G.; Lin, X.; Wang, A.; Eden, H. S.; Lee, S.; Zhang, G. X.; Chen, X. Y. HSA Coated Iron Oxide Nanoparticles as Drug Delivery Vehicles for Cancer Therapy. *Mol. Pharmaceutics* **2011**, *8*, 1669−1676.
(28) Yi, X.; Lian, X.; Dong, J.; Wan, Z.; Xia, C.; Song, X.; Fu, Y.; Gong, T.; Zhang, Z. Co-delivery of Pirarubicin and Paclitaxel by Human Serum Albumin Nanoparticles to Enhance Antitumor Effect and Reduce Systemic Toxicity in Breast Cancers. *Mol. Pharm.* **2015**, *12*, 4085−4098.
(29) Sebak, S.; Mirzaei, M.; Malhotra, M.; Kulamarva, A.; Prakash, S. Human serum albumin nanoparticles as an efficient noscapine drug delivery system for potential use in breast cancer: preparation and in vitro analysis. *Int. J. Nanomed.* **2010**, *5*, 525−532.
(30) Hsu, K. C.; Chen, Y. F.; Lin, S. R.; Yang, J. M. iGEMDOCK: a graphical environment of enhancing GEMDOCK using pharmacological interactions and post-screening analysis. *BMC Bioinf.* **2011**, *12*, No. S33.
(31) Chen, M.; Huang, J.; Yang, X.; Liu, B.; Zhang, W.; Huang, L.; Deng, F.; Ma, J.; Bai, Y.; Lu, R.; Huang, B.; Gao, Q.; Zhuo, Y.; Ge, J. Serum starvation induced cell cycle synchronization facilitates human somatic cells reprogramming. *PLoS One* **2012**, *7*, No. e28203.
(32) Lin, W.; Coombes, A. G.; Davies, M. C.; Davis, S. S.; Illum, L. Preparation of sub-100 nm human serum albumin nanospheres using a pH-coacervation method. *J. Drug Targeting* **1993**, *1*, 237−243.
(33) Chandran, P.; Kavalakatt, A.; Malarvizhi, G. L.; Vasanthakumari, D. R.; Retnakumari, A. P.; Sidharthan, N.; Pavithran, K.; Nair, S.; Koyakutty, M. Epigenetics targeted protein-vorinostat nanomedicine inducing apoptosis in heterogeneous population of primary acute myeloid leukemia cells including refractory and relapsed cases. *Nanomedicine* **2014**, *10*, 721−732.
(34) Nakamura, S.; Hirano, I.; Okinaka, K.; Takemura, T.; Yokota, D.; Ono, T.; Shigeno, K.; Shibata, K.; Fujisawa, S.; Ohnishi, K. The FOXM1 transcriptional factor promotes the proliferation of leukemia cells through modulation of cell cycle progression in acute myeloid leukemia. *Carcinogenesis* **2010**, *31*, 2012−2021.
(35) Fourneaux, B.; Bourdon, A.; Dadone, B.; Lucchesi, C.; Daigle, S. R.; Richard, E.; Laroche-Clary, A.; Le Loarer, F.; Italiano, A. Identifying and targeting cancer stem cells in leiomyosarcoma: prognostic impact and role to overcome secondary resistance to PI3K/mTOR inhibition. *J. Hematol. Oncol.* **2019**, *12*, No. 11.
(36) Rabinovitch, P. S.; Kubbies, M.; Chen, Y. C.; Schindler, D.; Hoehn, H. BrdU-Hoechst flow cytometry: a unique tool for quantitative cell cycle analysis. *Exp. Cell Res.* **1988**, *174*, 309−318.
(37) Rajendran, V.; Jain, M. V. In Vitro Tumorigenic Assay: Colony Forming Assay for Cancer Stem Cells. In *Cancer Stem Cells: Methods and Protocols*; Papaccio, G.; Desiderio, V., Eds.; Springer: New York, NY, 2018; pp 89−95.
(38) Kang, K. B.; Lawrence, B. D.; Gao, X. R.; Guaiquil, V. H.; Liu, A.; Rosenblatt, M. I. The Effect of Micro- and Nanoscale Surface Topographies on Silk on Human Corneal Limbal Epithelial Cell Differentiation. *Sci. Rep.* **2019**, *9*, No. 1507.
(39) Hwang-Verslues, W. W.; Kuo, W. H.; Chang, P. H.; Pan, C. C.; Wang, H. H.; Tsai, S. T.; Jeng, Y. M.; Shew, J. Y.; Kung, J. T.; Chen, C. H.; Lee, E. Y.; Chang, K. J.; Lee, W. H. Multiple lineages of human breast cancer stem/progenitor cells identified by profiling with stem cell markers. *PLoS One* **2009**, *4*, No. e8377.
(40) Pan, Y. M.; Wang, C. G.; Zhu, M.; Xing, R.; Cui, J. T.; Li, W. M.; Yu, D. D.; Wang, S. B.; Zhu, W.; Ye, Y. J.; Wu, Y.; Wang, S.; Lu, Y. Y. STAT3 signaling drives EZH2 transcriptional activation and mediates poor prognosis in gastric cancer. *Mol. Cancer* **2016**, *15*, No. 79.
(41) Kunderfranco, P.; Mello-Grand, M.; Cangemi, R.; Pellini, S.; Mensah, A.; Albertini, V.; Malek, A.; Chiorino, G.; Catapano, C. V.; Carbone, G. M. ETS transcription factors control transcription of EZH2 and epigenetic silencing of the tumor suppressor gene Nkx3.1 in prostate cancer. *PLoS One* **2010**, *5*, No. e10547.
(42) Ates, G. B.; Ak, A.; Garipcan, B.; Gulsoy, M. Indocyanine green-mediated photobiomodulation on human osteoblast cells. *Lasers Med. Sci.* **2018**, *33*, 1591−1599.
(43) Gryder, B. E.; Akbashev, M. J.; Rood, M. K.; Raftery, E. D.; Meyers, W. M.; Dillard, P.; Khan, S.; Oyelere, A. K. Selectively targeting prostate cancer with antiandrogen equipped histone deacetylase inhibitors. *ACS Chem. Biol.* **2013**, *8*, 2550−2560.
(44) Selvi, B. R.; Jagadeesan, D.; Suma, B. S.; Nagashankar, G.; Arif, M.; Balasubramanyam, K.; Eswaramoorthy, M.; Kundu, T. K. Intrinsically fluorescent carbon nanospheres as a nuclear targeting vector: delivery of membrane-impermeable molecule to modulate gene expression in vivo. *Nano Lett.* **2008**, *8*, 3182−3188.
(45) Jiang, Y.; Wong, S.; Chen, F.; Chang, T.; Lu, H.; Stenzel, M. H. Influencing Selectivity to Cancer Cells with Mixed Nanoparticles Prepared from Albumin-Polymer Conjugates and Block Copolymers. *Bioconjugate Chem.* **2017**, *28*, 979−985.
(46) Frei, E. Albumin binding ligands and albumin conjugate uptake by cancer cells. *Diabetol. Metab. Syndr.* **2011**, *3*, No. 11.
(47) Requirand, G.; Robert, N.; Boireau, S.; Vincent, L.; Seckinger, A.; Bouhya, S.; Ceballos, P.; Cartron, G.; Hose, D.; Klein, B.; Moreaux, J. BrdU incorporation in multiparameter flow cytometry: A new cell cycle assessment approach in multiple myeloma. *Cytometry, Part B* **2019**, *96*, 209−214.
(48) Strom, D. K.; Nip, J.; Westendorf, J. J.; Linggi, B.; Lutterbach, B.; Downing, J. R.; Lenny, N.; Hiebert, S. W. Expression of the AML-1 oncogene shortens the G(1) phase of the cell cycle. *J. Biol. Chem.* **2000**, *275*, 3438−3445.
(49) O'Meara, M. M.; Simon, J. A. Inner workings and regulatory inputs that control Polycomb repressive complex 2. *Chromosoma* **2012**, *121*, 221−234.
(50) Crowley, L. C.; Waterhouse, N. J. Measuring Survival of Hematopoietic Cancer Cells with the Colony-Forming Assay in Soft Agar. *Cold Spring Harbor Protocols* **2016**, *2016*, No. pdb.prot087189.
(51) Momparler, R. L.; Cote, S.; Momparler, L. F.; Idaghdour, Y. Epigenetic therapy of acute myeloid leukemia using 5-aza-2′-deoxycytidine (decitabine) in combination with inhibitors of histone methylation and deacetylation. *Clin. Epigenet.* **2014**, *6*, No. 19.
(52) Ko, B. S.; Lu, Y. J.; Yao, W. L.; Liu, T. A.; Tzean, S. S.; Shen, T. L.; Liou, J. Y. Cordycepin regulates GSK-3beta/beta-catenin signaling in human leukemia cells. *PLoS One* **2013**, *8*, No. e76320.
(53) Bernas, T.; Dobrucki, J. Mitochondrial and nonmitochondrial reduction of MTT: interaction of MTT with TMRE, JC-1, and NAO mitochondrial fluorescent probes. *Cytometry* **2002**, *47*, 236−242.
(54) Chen, J. C.; Zhang, X.; Singleton, T. P.; Kiechle, F. L. Mitochondrial membrane potential change induced by Hoechst 33342 in myelogenous leukemia cell line HL-60. *Ann. Clin. Lab. Sci.* **2004**, *34*, 458−466.
(55) Ross Levine, L. L.; Omar, A.-W. Biomarkers for Response to EZH2 Inhibitors. US Patent Application Publication, May 18, 2017.

DOI: 10.1021/acs.molpharmaceut.9b01071
Mol. Pharmaceutics XXXX, XXX, XXX−XXX

(56) Laugesen, A.; Hojfeldt, J. W.; Helin, K. Role of the Polycomb Repressive Complex 2 (PRC2) in Transcriptional Regulation and Cancer. *Cold Spring Harbor Perspect. Med.* **2016**, *6*, No. a026575.
(57) Kawano, S.; Grassian, A. R.; Tsuda, M.; Knutson, S. K.; Warholic, N. M.; Kuznetsov, G.; Xu, S.; Xiao, Y.; Pollock, R. M.; Smith, J. S.; Kuntz, K. K.; Ribich, S.; Minoshima, Y.; Matsui, J.; Copeland, R. A.; Tanaka, S.; Keilhack, H. Preclinical Evidence of Anti-Tumor Activity Induced by EZH2 Inhibition in Human Models of Synovial Sarcoma. *PLoS One* **2016**, *11*, No. e0158888.
(58) Girard, N.; Bazille, C.; Lhuissier, E.; Benateau, H.; Llombart-Bosch, A.; Boumediene, K.; Bauge, C. 3-Deazaneplanocin A (DZNep), an inhibitor of the histone methyltransferase EZH2, induces apoptosis and reduces cell migration in chondrosarcoma cells. *PLoS One* **2014**, *9*, No. e98176.
(59) Fisher, M. L.; Adhikary, G.; Grun, D.; Kaetzel, D. M.; Eckert, R. L. The Ezh2 polycomb group protein drives an aggressive phenotype in melanoma cancer stem cells and is a target of diet derived sulforaphane. *Mol. Carcinog.* **2016**, *55*, 2024−2036.
(60) Khan, N.; Bharali, D. J.; Adhami, V. M.; Siddiqui, I. A.; Cui, H.; Shabana, S. M.; Mousa, S. A.; Mukhtar, H. Oral administration of naturally occurring chitosan-based nanoformulated green tea polyphenol EGCG effectively inhibits prostate cancer cell growth in a xenograft model. *Carcinogenesis* **2014**, *35*, 415−423.
(61) Li, Z.; Wang, Y.; Qiu, J.; Li, Q.; Yuan, C.; Zhang, W.; Wang, D.; Ye, J.; Jiang, H.; Yang, J.; Cheng, J. The polycomb group protein EZH2 is a novel therapeutic target in tongue cancer. *Oncotarget* **2013**, *4*, 2532−2549.
(62) Choudhury, S. R.; Balasubramanian, S.; Chew, Y. C.; Han, B.; Marquez, V. E.; Eckert, R. L. (-)-Epigallocatechin-3-gallate and DZNep reduce polycomb protein level via a proteasome-dependent mechanism in skin cancer cells. *Carcinogenesis* **2011**, *32*, 1525−1532.
(63) Walf-Vorderwülbecke, V.; Pearce, K.; Brooks, T.; Hubank, M.; van den Heuvel-Eibrink, M. M.; Zwaan, C. M.; Adams, S.; Edwards, D.; Bartram, J.; Samarasinghe, S.; Ancliff, P.; Khwaja, A.; Goulden, N.; Williams, G.; de Boer, J.; Williams, O. Targeting acute myeloid leukemia by drug-induced c-MYB degradation. *Leukemia* **2018**, *32*, 882.
(64) Calabretta, B.; Sims, R. B.; Valtieri, M.; Caracciolo, D.; Szczylik, C.; Venturelli, D.; Ratajczak, M.; Beran, M.; Gewirtz, A. M. Normal and leukemic hematopoietic cells manifest differential sensitivity to inhibitory effects of c-myb antisense oligodeoxynucleotides: an in vitro study relevant to bone marrow purging. *Proc. Natl. Acad. Sci. U.S.A.* **1991**, *88*, 2351−2355.
(65) Waldron, T.; De Dominici, M.; Soliera, A. R.; Audia, A.; Iacobucci, I.; Lonetti, A.; Martinelli, G.; Zhang, Y.; Martinez, R.; Hyslop, T.; Bender, T. P.; Calabretta, B. c-Myb and its target Bmi1 are required for p190BCR/ABL leukemogenesis in mouse and human cells. *Leukemia* **2012**, *26*, 644−653.
(66) Li, H.; Xu, J.; Zhou, Y.; Liu, X.; Shen, L. E.; Zhu, Y. U.; Li, Z.; Wang, X.; Guo, Q.; Hui, H. PLSCR1/IP3R1/Ca(2+) axis contributes to differentiation of primary AML cells induced by wogonoside. *Cell Death Dis.* **2017**, *8*, No. e2768.

DOI: 10.1021/acs.molpharmaceut.9b01071
Mol. Pharmaceutics XXXX, XXX, XXX−XXX